

Article

Abiogenesis on Different Star Types; a Dissipative Photochemical Perspective

Andrés Ledesma¹ and Karo Michaelian² 

[1] Faculty of Science, Universidad Nacional Autónoma de México, Circuito Interior de la Investigación Científica, Ciudad Universitaria, Ciudad de México, C.P. 04510.; andreslr@ciencias.unam.mx

[2] Department of Nuclear Physics and Application of Radiation, Instituto de Física, Universidad Nacional Autónoma de México, Circuito Interior de la Investigación Científica, Ciudad Universitaria, Ciudad de México, C.P. 04510.; karo@fisica.unam.mx

* karo@fisica.unam.mx

Abstract: The “thermodynamic dissipation theory for the origin of life” asserts a thermodynamic imperative for the origin of life, suggesting that the fundamental molecules of life originated as self-organized molecular photon dissipative structures (chromophores or pigments) that proliferated over the ocean surface to absorb and dissipate into heat the Archean solar “soft” UV-C (205–285 nm) and UV-B light (< 320 nm) of our G-type star. Gradually, under this thermodynamic imperative, more complex biosynthetic pathways, like extant photosynthesis, emerged to dissipate the less energetic but higher intensity UV-A and visible light. Thermodynamic coupling to other antenna and ocean surface anchoring molecules, as well as to abiotic dissipative processes such as the water cycle and wind and ocean currents, led to today’s biosphere, dissipating the incident solar spectrum well into the infrared. Shorter wavelength “hard” UV-C light (< 205 nm) may, depending on atmospheric conditions, have reached Earth’s surface and ionized and dissociated or otherwise degraded these carbon-based pigment molecules (as probably occurred on Mars after losing most of its atmosphere). Here we assess the possibility for an abiogenesis of life similar to ours through molecular photon dissipative structuring on planets similar to early Earth but orbiting different star types at distances normalized to the solar constant. Emission spectra of star types are analyzed to determine the ratio of integrated photon fluxes in the soft UV-C wavelength (dissipative structuring) to hard UV-C wavelength (degradation) regions. Our analysis suggests that star types favorable to the dissipative structuring of life, potentially evolving towards complex life forms such as bacteria, are only the F, G and high mass K-types, with intelligent life only possible on G-type stars. Low mass K and M-type stars are highly unlikely to harbor life. Biosignatures related to the thermodynamic imperative of photon dissipation are proposed.



Citation: Ledesma, A.; Michaelian, K. Abiogenesis on Different Star Types. *Preprints* **2022**, *1*, 0. <https://doi.org/>

Publisher’s Note: MDPI stays neutral with regard to jurisdictional claims in published maps and institutional affiliations.



Copyright: © 2022 by the authors. Licensee MDPI, Basel, Switzerland. This article is an open access article distributed under the terms and conditions of the Creative Commons Attribution (CC BY) license (<https://creativecommons.org/licenses/by/4.0/>).

Keywords: origin of life; dissipative structuring; prebiotic chemistry; abiogenesis; astrobiology; non-equilibrium thermodynamics; thermodynamic dissipation theory; ionization; dissociation; star types; biosignatures

MSC: 92B05, 85A20, 92D99, 92C05, 92C15, 92C40, 92C45, 80Axx, 82Cxx, 82B35, 82C26

1. Introduction

Our Sun, a G-type star, harbors a planet with carbon-based life. G-type stars, however, make up less than 7% of stars in our galaxy. An important question is therefore whether other star types could also harbor similar carbon-based life? A decisive answer to this question, of course, depends on knowing the particular chemical and physical processes which gave rise to the origin of life on Earth some 3.85 billion years ago. A contemporary theory gaining increasing acceptance, the “Thermodynamic Dissipation Theory for the Origin of Life” (TDTOL) [1–20], argues that the origin of life was a photochemical molecular dissipative structuring process giving rise to the fundamental molecules of life as UV-C chromophores for dissipating this light into heat. This could only occur on planetary surfaces exposed to soft UV-C light of 205–285 nm and UV-B light (< 320 nm). Shorter wavelengths could ionize and dissociate, or otherwise degrade, these carbon-based molecules,

while wavelengths longer than 285 nm would not have sufficient energy to transform most organic double covalent molecular bonds. Wavelengths longer than 320 nm would not have sufficient energy to transform most single covalent bonds and therefore could not be involved in direct molecular dissipative structuring.

Significant evidence suggests that the origin of life concerned not only chemical reactions (thermally or catalytically activated) but also photochemical reactions [2,21,22], including perhaps a UV selection processes [23–26]. More emphatically, we have proposed [1,2,7–9,15,20] that the fundamental molecules of life were originally UV-C chromophores formed through molecular dissipative structuring from common simple precursors such as hydrogen cyanide (HCN), cyanogen (NCCN) and carbon dioxide (CO₂) in water solvent under the surface UV-C light environment of the early Archean.

TDTOL asserts that the dissipative structuring of organic chromophores under light is the fundamental creative force in biology, ongoing since the initial direct molecular dissipative structuring at UV-C wavelengths of the early Archean, giving rise to the fundamental molecules of life – the UV-C pigments of the Archean – to the more complex, but still dissipatively structured, biosynthetic pathway known as “photosynthesis” at visible wavelengths up to the red edge (~ 700 nm), giving rise to the visible pigments of today [19].

The coupling of the photon dissipative process within the organic pigments of plants and cyanobacteria with animal husbandry of these, and with abiotic irreversible processes such as the water cycle and ocean and atmospheric currents, further increased the efficacy of solar photon dissipation into the infrared, culminating in an efficient global photon dissipating system known as the biosphere.

If dissipative structuring of carbon based organic pigments under UV-C light is indeed the correct theory of abiogenesis (see section 4 for evidence), then a very particular region of the electromagnetic spectrum at a planet surface, limited on the long-wavelength side by the strength of molecular covalent bonding and on the short wavelength side by molecular ionization energies, is required for abiogenesis.

The aim of this paper is to determine which star types are conducive to providing this light environment and thereby identify which of these stars could support an origin of life similar to our own. We consider only planets similar to Earth orbiting their star type at a distance corresponding to its habitable zone, where its stellar constant equals our solar constant. This latter requirement ensures the possibility of water in its liquid state and similar chemical reaction rates.

The search for extraterrestrial life has particular relevance now that a number of space-based telescopes are scanning extra-solar planets for biosignatures. Time on these telescopes is at a premium and it is thus important to optimize the selection for observation stars-planet combinations with high probability for harboring life similar to ours, and, indeed, knowing what biosignatures best to look for.

2. The Early Archean

Early Archean surface O₂ levels were less than 10^{-6} times present values while N₂ levels were similar to today's or possibly a few times lower. CO₂ and CH₄ levels ranged from ~ 10 to 2500 and 10^2 to 10^4 times modern amounts, respectively [27–29]. Greenhouse gas concentrations were sufficient to offset an approximately 25% fainter Sun. A faster rotating Earth (~ 14 hour rotational period) meant a greater latitudinal gradient in surface temperature [30] which may have ranged from $\sim 90^\circ\text{C}$ at the equator [31–33] to 0°C at the poles [29].

Hydrogen cyanide (HCN) was recognized over a century ago as a likely precursor of life's fundamental molecules [34], in particular for the nucleobases [15]. The formation of HCN in an N₂-rich atmosphere requires first breaking the triple covalent bond between nitrogens, N≡N, and then atomic nitrogen attacking a carbon atom. Given the atmospheric abundance of N₂ and a carbon to oxygen ratio of C/O ≥ 1 of the early Archean, this can be accomplished readily via photochemistry [35]. N₂ absorbs strongly between approximately

120 to 145 nm. The N_2 photodissociation energy ~ 9.8 eV corresponds to a wavelength of 126.5 nm (close to the solar Lyman- α line of 121 nm).

The removal of a proton from HCN in neutral water requires a photon of about 238.4 nm (5.2 eV) while its photodissociation energy is about 93 nm (13.3 eV). HCN absorbs most strongly at ~ 150 nm (8.27 eV). It has been estimated that HCN concentrations as high as 6×10^{-5} M may have been common in the enriched microlayer of the Archean ocean surface [15].

3. The Thermodynamic Dissipation Theory for the Origin and Evolution of Life

The dissipative structuring of material under an externally imposed thermodynamic potential is a well-understood non-equilibrium thermodynamic phenomenon which explains physical-chemical processes arising “spontaneously” to increase the dissipation of the imposed potential [36]. The Thermodynamic Dissipation Theory for the Origin of Life (TDTOL) [1–20] identifies this generalized thermodynamic potential for the dissipative structuring involved in the origin of life as the solar photon potential of soft UV-C wavelengths between 205 and 285 nm as well as the UV-B up to 320 nm. In this region, photons can transform covalent bonds of carbon-based molecules but rarely cause molecular dissociation through ionization. Few photons of wavelength < 205 nm and between 285 and 305 nm reached Earth’s surface during the Archean due to absorption by atmospheric gases; principally CO_2 , N_2 and the aldehydes, respectively [23]. This photon potential was available at Earth’s surface before the origin of life (~ 3.9 Ga) and persisted for at least 1200 million years thereafter until after the emergence of oxygenic photosynthesis and an ensuing UV “protective” ozone layer at about 2.7 Ga [23,37].

The TDTOL proposes that the fundamental molecules of life (those in the three domains of life - nucleic acids, amino acids, fatty acids, sugars, cofactors, etc.) were initially UV-C chromophores, dissipatively structured on the ocean surface under the mentioned UV-C photon potential from common precursors such as hydrogen cyanide (HCN) and its derivatives such as cyanogen (NCCN), carbon dioxide (CO_2), and water [9,12,15,17,18]. Prebiotic vesicles, themselves being photon dissipative and hard UV-C protective structures [12,38], would form naturally at the ocean surface from photon-dissipatively structured fatty acids [12] and isoprenes, through surface agitation and Gibb’s free energy minimization.

4. Evidence for a Photochemical Dissipative Origin of Life

Empirical evidence supports our assertion that the fundamental molecules of life were dissipatively structured as UV-C chromophores (the “Pigment World” hypothesis [2,20]) at the origin of life:

1. All non-equilibrium processes are driven by a source of free energy. The free energy available in UV light of wavelength less than 320 nm arriving at Earth’s surface today is more than 1000 times greater than that of all other non-photon energy sources combined [39], and this would have been even greater during the Archean because of the lack of an atmospheric ozone layer.
2. The wavelength of maximum absorption of many of the fundamental molecules coincide with the predicted UV-C window in the Archean atmosphere (Fig. 1) and this coincides neatly with the spectral region (~ 205 – 285 nm) required for dissipative structuring.
3. Many of the fundamental molecules of life are endowed with *peaked conical intersections* giving them broad band absorption and large quantum efficiency for internal conversion, i.e. extremely rapid (sub-picosecond) dissipation of the photon-induced electronic excitation energy into vibrational energy of molecular atomic coordinates, and finally into the surrounding water solvent [9,15,40]. It is the photon-induced excitation of an electron into an anti-bonding orbital (e.g., $\pi \rightarrow \pi^*$) that weakens the respective bond, decreasing the energy of the excited state upon elongation of the

bond, leading to intersection of the excited state potential energy surface with that of the electronic ground state (Fig. 3).

4. Even minor transformations (e.g., protonations, tautomerizations or methylations) of the fundamental molecules of life, which often, in fact, endows them with lower Gibb's free energy, eliminates completely, or significantly reduces, their extraordinary photon absorption and dissipation properties [41].
5. The wavelength of maximum absorption of the fundamental molecules can be tuned simply by a protonation or deprotonation event (changing the conjugation number), decreasing or increasing, respectively, this wavelength by about 30 nm (Fig. 2). This allows photon dissipative chromophores to easily evolve towards dissipation of the higher intensity light at longer wavelengths and thereby thermodynamically "adapt" towards dissipation of the most potent, or changing, surface solar spectrum.
6. Many photochemical routes, from common and simple Archean precursor molecules, to the synthesis of nucleic acids [21], amino acids [42], fatty acids [12], sugars [43,44], and other pigments [7,45] have been identified at these UV-C wavelengths.
7. The rate of photon dissipation within the Archean UV-C window generally increases after each incremental transformation on route to photochemical synthesis of the fundamental molecule (Fig. 4), and this is a hallmark of dissipative structuring in the non-equilibrium thermodynamic regime [9,12,15].

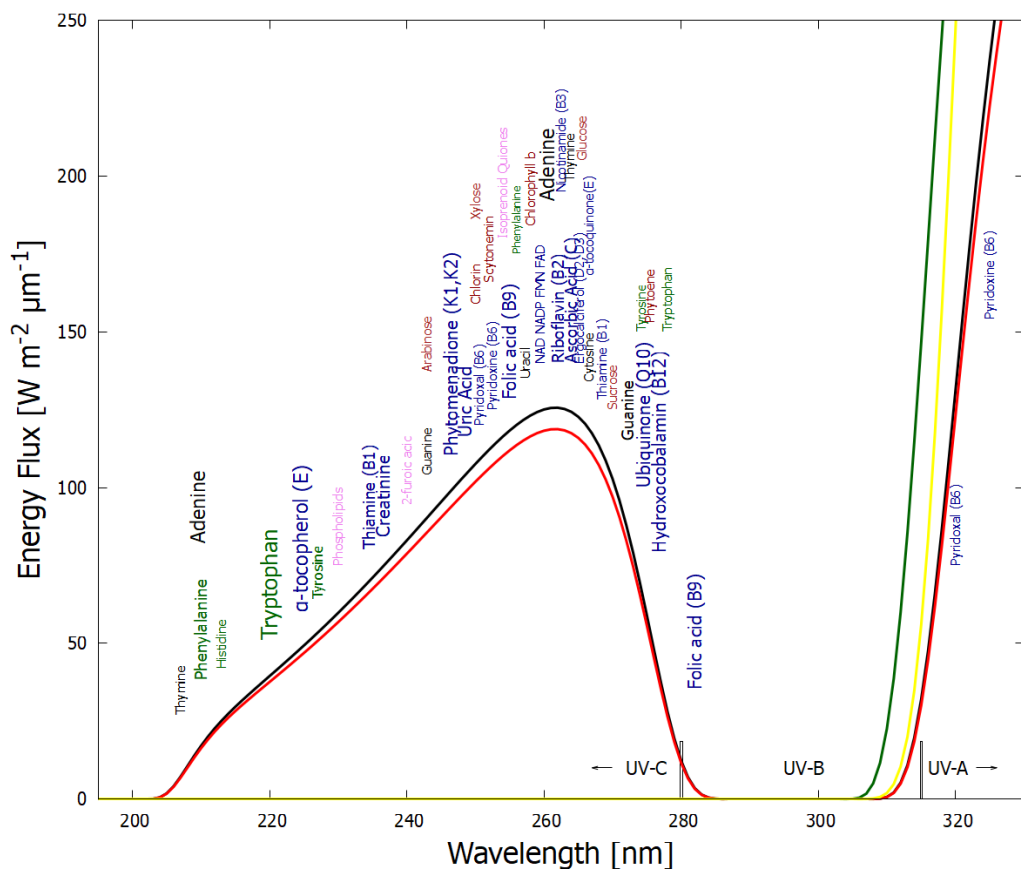


Figure 1. The spectrum of UV light available at Earth's surface before the origin of life at approximately 3.9 Ga and until at least 2.9 Ga (curves black and red, respectively). This spectrum in the UV-C may even have persisted throughout the entire Archean until 2.5 Ga [46]. Atmospheric CO₂, H₂O, SO₂ and probably some H₂S, were responsible for the absorption of wavelengths shorter than ~ 205 nm, and atmospheric aldehydes (e.g., formaldehyde and acetaldehyde, common photochemical products of CO₂ and water) absorbed between about 285 and 305 nm [23,47]), approximately corresponding to the UV-B region (280 and 315 nm). By around 2.2 Ga (green curve), UV-C light at Earth's surface was completely extinguished by the pigments of oxygen and ozone resulting from organisms performing oxygenic photosynthesis. The yellow curve corresponds to the present surface spectrum. Energy fluxes are for the Sun at the zenith. Over 50 of the fundamental molecules of life are plotted at their wavelengths of maximum absorption: nucleic acids (black), amino acids (green), fatty acids (violet), sugars (brown), vitamins, co-enzymes, and cofactors (blue), and pigments (red). We have asserted that these molecules were dissipatively structured as UV-C pigments under this light. The font size is roughly proportional to the relative size of the respective molar extinction coefficient of the pigment. Adapted with permission from Michaelian and Simeonov [7].

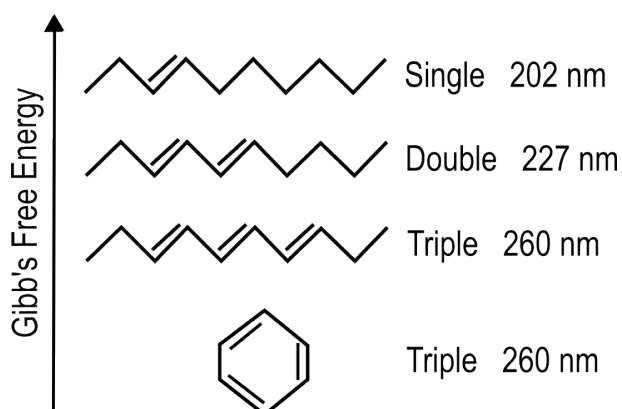


Figure 2. Conjugated carbon molecules are more stable (lower Gibb's free energy in the ground state) as compared to saturated molecules, but more importantly provide new collective electron orbitals giving rise to excited states at energies adequate for the absorption of soft UV-C photons. The greater the conjugation number, the greater the wavelength of maximum absorption. The wavelength of maximum absorption of the chromophore can, therefore, be tuned simply by a protonation or deprotonation event. Conjugation is also important for giving molecules a conical intersection (Fig. 3) allowing rapid dissipation of the electronic excited state energy into heat (internal conversion). Photon dissipation is the thermodynamic reason for the occurrence of organic molecules in nature. Reprinted with permission from Michaelian [9].

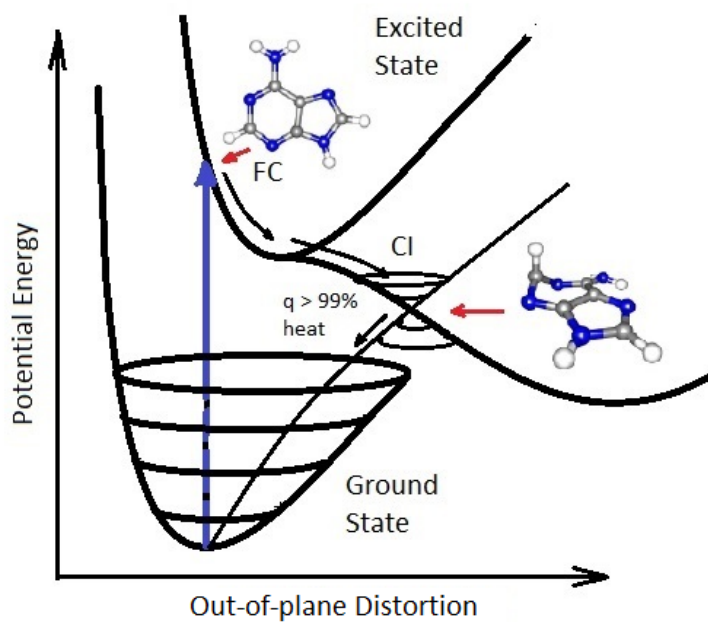


Figure 3. A conical Intersection (CI) for excited adenine showing a degeneracy of the electronic excited state with the vibrational states superimposed on the electronic ground state after a UV-C photon absorption event (blue arrow) which induces a nuclear coordinate deformation from the molecules original planer structure in the Franck-Condon (FC) region to activation of an N9-H stretch or a ring-puckering motion known as *pyramidalization* (shown in the diagram). The most probable deformation depends on the incident photon energy and protonation state. It is this deformation, resulting from excitation of an anti-bonding state (e.g., $\pi \rightarrow \pi^*$), which leads to a lowering of the excited potential energy surface such that it intersects with vibrational states of the electronic ground state, resulting in the conical intersection. Conical intersections provide rapid (sub-picosecond) dissipation of the electronic excitation energy into vibrational energy (heat). The quantum efficiency, q , for this dissipative route is very large ($> 99\%$) for many of the fundamental molecules of life, making them photochemically stable and, more importantly (from our thermodynamic perspective), very efficient at UV-C photon dissipation. Another common form of coordinate transformation mediated through conical intersections are proton and electron transfers within the molecule or with the solvent environment and this may have relevance to enzyme-less photon-induced denaturing of RNA and DNA [13] and to photosynthesis [45]. The diagram is based on data from Andrew Orr-Ewing [48], Roberts et al. [49], Kleinermanns et al. [50], and Barbatti et al. [51]). Reprinted with permission from Michaelian [15].

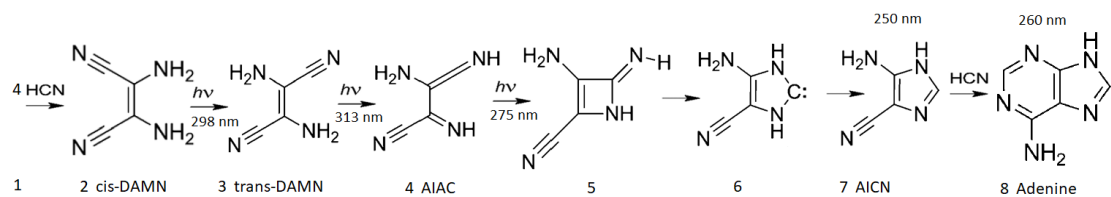


Figure 4. The photochemical dissipative structuring of adenine from 5 molecules of hydrogen cyanide (HCN) in water, first observed by Ferris and Orgel (1966) [21,52]. Four molecules of HCN (1) are transformed into the smallest stable oligomer (tetramer) of HCN, known as cis-2,3-diaminomaleonitrile (cis-DAMN) (2), which, under a constant UV-C photon flux, isomerizes into trans-DAMN (3) (also known as diaminofumaronitrile, DAFN) which can be converted, on absorbing two more UV-C photons, into an imidazole intermediate, 4-amino-1H-imidazole-5-carbonitrile (AICN) (7). Hot ground state thermal reactions with another HCN molecule or its hydrolysis product formamide (or ammonium formate) leads to the purine adenine (8). This is a microscopic dissipative structuring process which ends in adenine [9,15], a UV-C pigment with a large molar extinction coefficient at the maximum intensity of the UV-C Archean surface solar spectrum (260 nm - Figs. 1) and a peaked conical intersection facilitating rapid dissipation of photons at these wavelengths. The other nucleobases have similar optical characteristics and also appear to be UV-C molecular dissipative structures (e.g., reference [18] and figure 5). Reprinted with permission from Michaelian [15].

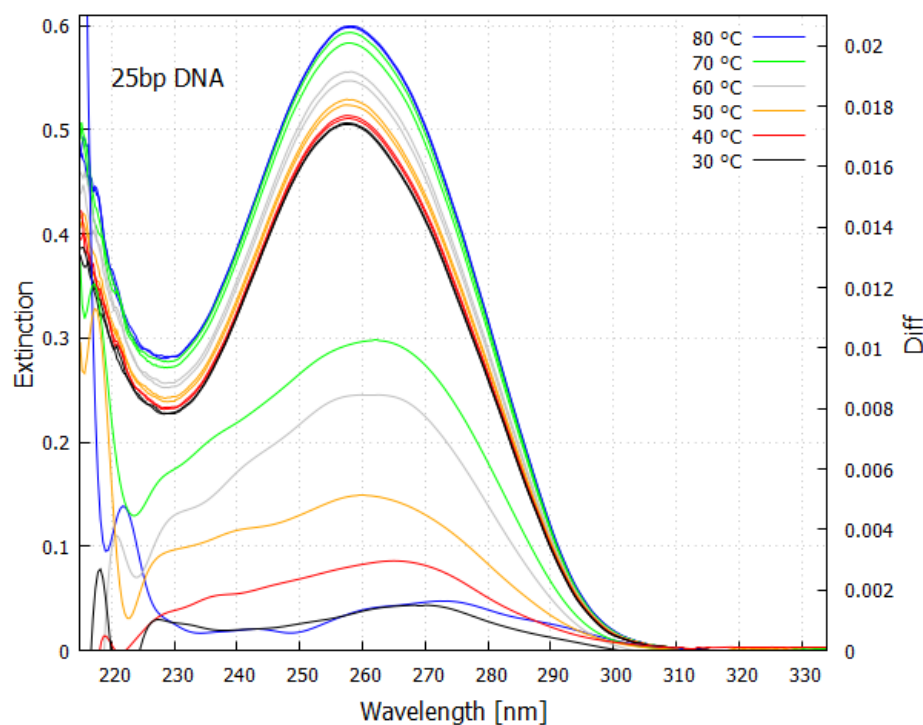


Figure 5. Absorption spectrum of 25bp DNA (including all DNA nucleobases) in the soft UV-C region showing hyperchromism resulting from the denaturing with temperature. The lower curves are the thermal difference spectra (right y-axis) obtained by subtracting the lower temperature extinction curve from the higher temperature curve for a 3 °C bin centered at the specified temperature (smoothed with a 2000 point Bezier function). Peak absorption at ~260 nm corresponds to the peak in the incident UV-C spectrum arriving at Earth's surface during the Archean (Fig. 1). Large broadband absorption implies rapid (sub-picosecond) dissipation of the electronic excitation energy into heat through conical intersections (Fig. 3). Reprinted with permission from Michaelian and Santillan [13].

Such extraordinary photochemical properties of the fundamental molecules cannot be considered as mere coincidences, but rather as expected attributes of molecular dissipative structuring in this UV-C spectral region.

5. Molecular Ionization and Dissociation

Persistent dissipative structuring requires the exclusion of photon wavelengths shorter than approximately 205 nm where ionization leading to molecular degradation could occur. The Earth's Archean surface spectrum, in fact, had few photons of wavelength shorter than about 205 nm (Figs. 1 and 9) since these are strongly absorbed by atmospheric N₂, CO₂, H₂S and H₂O, but this is not necessarily the case for similar planets on other star types.

Ionization energies (IEs) listed in table 1 of some of the important fundamental molecules in water at neutral pH were obtained from published gas phase values by applying a solvation correction which decreases IEs due to stabilization of the cation radical by the polar solvent. Studies suggest a 1.5–2 eV reduction for neutral bases [53] and amino acids [54], and 3–5 eV for nucleotides (with phosphates). Here we use a ~1.9 eV shift for nucleobases (without phosphates) and amino acids, ~2.0 eV for sugars ([55] - interpolated from polyol studies), reflecting typical small-molecule solvation [56]. At neutral pH, amino acids exist as zwitterions (except histidine's imidazole, which is partially protonated) and nucleic bases are neutral.

Short and medium-chain fatty acid IEs in water are derived from gas-phase data (acetic, butyric) and trends (caprylic, capric), reduced by ~1.5 eV for aqueous anionic forms. Long-chain saturated fatty acid IEs are estimated from chain-length trends and reduced by ~1.5 eV in water. The ~1.5 eV reduction approximates deprotonation (~1 eV) and solvation (~0.5 eV), but actual shifts vary (± 0.5 – 1 eV). For the triple conjugated fatty acids, the IEs are estimated ~0.4–0.6 eV lower than stearic acid's gas-phase value due to conjugation, then further reduced by ~1.5 eV. Slight variations reflect cis/trans effects (all-trans β -eleostearic fatty acids are lowest).

Table 1. Estimated aqueous ionization energies (IEs) of nucleic acids, amino acids, sugars and fatty acids in water at pH 7, along with corresponding photon wavelengths (λ). The values listed are approximate, obtained from gas-phase experimental data adjusted by typical solvation shifts assuming neutral (pH 7) and physiological forms (zwitterions for amino acids and neutral bases). Charged states (e.g., deprotonated cysteine) could shift IEs further. Nucleobases are listed alone, not as nucleotides, and sugars are free, not in polymers. Including phosphates or glycosidic bonds would lower IEs further (e.g., AMP \sim 4.5 eV).

Molecule	IEs (eV)	λ (nm)
<i>Nucleic Acid Bases</i>		
Adenine	6.5	190
Cytosine	6.7	185
Guanine	6.0	207
Thymine	6.9	180
Uracil	7.1	175
<i>Selected Amino Acids</i>		
Alanine	7.7	161
Cysteine	6.4	194
Glycine	7.6	163
Histidine	6.8	182
Tryptophan	7.3	170
Tyrosine	6.5	190
<i>Sugars</i>		
Ribose	7.5	165
Deoxyribose	7.5	165
Glucose	7.7	161
Fructose	7.6	163
<i>Fatty Acids</i>		
Short-Chain		
Acetic Acid (C2:0)	9.2	135
Butyric Acid (C4:0)	8.7	143
Medium-Chain		
Caprylic Acid (C8:0)	8.3	149
Capric Acid (C10:0)	8.2	151
Long-Chain		
Palmitic Acid (C16:0)	8.0	155
Stearic Acid (C18:0)	7.9	157
α -Eleostearic Acid (C18:3, 9c,11t,13t)	7.4	168
β -Eleostearic Acid (C18:3, 9t,11t,13t)	7.4	169
Punicic Acid (C18:3, 9c,11t,13c)	7.4	166

All fundamental molecules listed in table 1 have higher ionization energies than the short wavelength cut-off of Earth's Archean surface spectrum (\sim 205 nm - Fig. 1). Guanine is close to the edge at 207 nm.

6. Star Type Spectral Outputs

Table 2 lists the stellar parameters of main-sequence O, B, A, F, G, K, M-type, luminosity class V, stars with planet-star distances normalized to the solar constant of 1366 W/m^2 . The calculations use standard astronomical constants: $\sigma = 5.670367 \times 10^{-8} \text{ W/m}^2/\text{K}^4$, solar surface temperature 5772 K, and solar radius (R_\odot).

Table 2. Stellar parameters and energy and photon fluxes at the top of the atmosphere for a planet like Earth at a distance from its star normalized to the solar constant of 1366 W m^{-2} . The columns are; star type, surface temperature, radius of star with respect to that of the Sun (R_{\odot}), planet habitable distance d , wavelength of maximum energy flux λ_{max}^E (nm), energy flux at maximum F_E ($\text{W/m}^2/\text{s}/\mu\text{m}$), wavelength of maximum photon number flux λ_{max}^P (nm), and photon number flux at maximum F_P ($\text{ph/m}^2/\text{s}/\mu\text{m}$).

Type	T (K)	$R (R_{\odot})$	d (au)	λ_{max}^E (nm)	F_E ($\text{W/m}^2/\text{s}/\mu\text{m}$)	λ_{max}^P (nm)	F_P ($\text{ph/m}^2/\text{s}/\mu\text{m}$)
O7 V	30 000	6.60	178.3	96.6	7866	122.3	4.21×10^{21}
B2 V	20 000	4.19	50.31	144.9	5244	183.5	4.21×10^{21}
A2 V	9000	1.86	4.515	322.0	2360	407.7	4.21×10^{21}
F5 V	6500	1.39	1.763	445.8	1705	564.6	4.21×10^{21}
G2 V	5772	1.00	1.000	502.0	1507	635.8	4.21×10^{21}
K2 V	5000	0.673	0.5051	579.6	1312	733.9	4.21×10^{21}
M2 V	3500	0.243	0.0892	827.9	918.7	1048.5	4.21×10^{21}

The star types (O, B, A, F, G, K, M) represent main-sequence stars. Once on the main sequence, the emitted spectrum of a star remains relatively stable for most of its lifetime and depends on its mass and metallicity. Temperatures are typical effective temperatures for mid-range subtypes of main-sequence stars [57]. Radii are typical for main-sequence stars and matched to the temperatures.

Planet-star distances d (au), are obtained by integrating the energy flux and equating it to the solar constant (1366 W/m^2), or more easily obtained from,

$$\sigma T^4 \left(\frac{R}{d} \right)^2 = 1366$$

giving,

$$d_{\text{au}} = \left(\frac{R}{R_{\odot}} \right) \cdot \left(\frac{T}{5772} \right)^2.$$

The electromagnetic spectrum emitted by bodies in thermal equilibrium is given by Planck's blackbody radiation equation and depends only on the temperature T . As a function of wavelength λ , the energy density (energy per unit volume per unit wavelength interval $d\lambda$) has the following form,

$$u(\lambda)d\lambda = \frac{8\pi hc}{\lambda^5(e^{\beta hc/\lambda} - 1)}d\lambda, \quad (1)$$

giving the amount of energy radiated between wavelengths $\lambda + d\lambda$ in a unit volume, with $\beta = 1/kT$.

This energy distribution $u(\lambda)$ has a maximum as a function of temperature as determine by Wien's displacement law,

$$\lambda_{max,E} = \frac{b}{T}, \quad (2)$$

where $\lambda_{max,E}$ (nm) represents the wavelength at which the peak of maximum emission occurs. T is the absolute temperature of the object in units of K, and $b = 2.8978 \times 10^6$ is the proportionality constant known as Wien's constant.

The spectral energy flux at $\lambda_{max,E}$ ($\text{W/m}^2/\mu\text{m}$) is computed using the Planck function, normalized to the planet distance,

$$F(\lambda_{\text{nm}}) = \frac{3.131 \times 10^{23}}{\lambda_{\text{nm}}^5} \frac{1}{e^{1.438776877 \times 10^7 / (\lambda_{\text{nm}} T)} - 1} \frac{1366}{\sigma T^4}$$

where $\lambda_{\text{nm}} = 2.8978 \times 10^6 / T$. The constant ensures F equals the solar output ($\approx 1507 \text{ W/m}^2/\mu\text{m}$) for a G2 V star (Sun) at 502 nm.

In figure 6, the planet-star distance normalized spectral energy flux $F(\lambda_{\text{nm}})$ is plotted over the wavelength region 0–2000 nm for all star types.

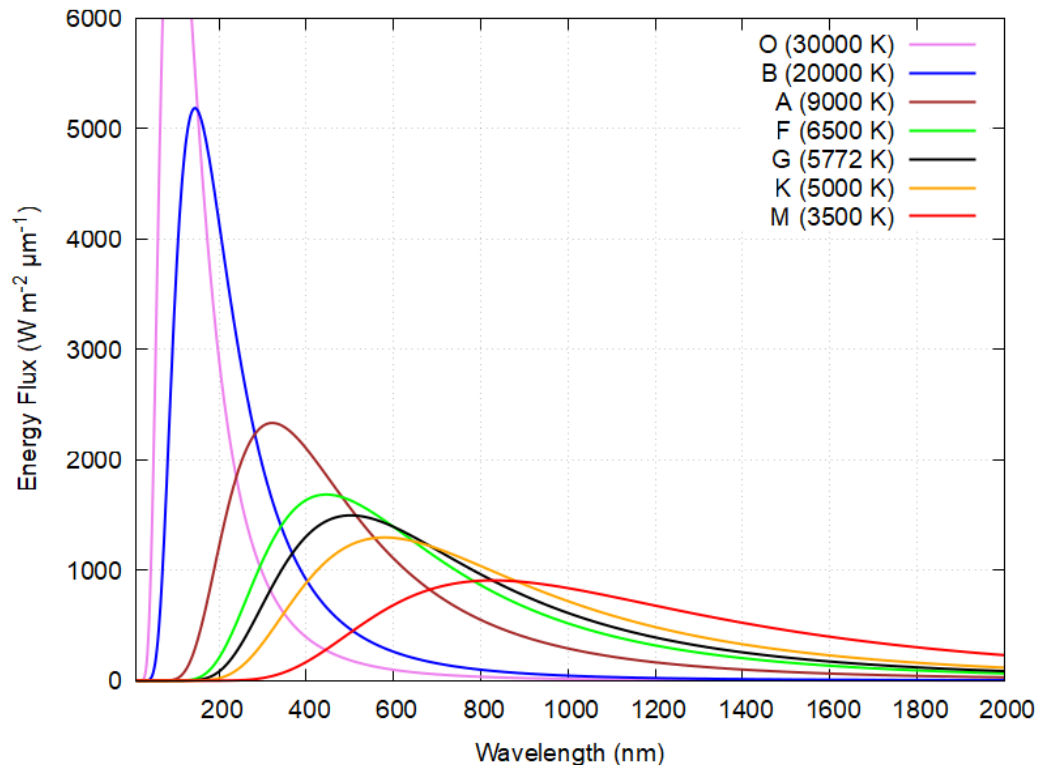


Figure 6. The energy fluxes of different star types at the top of the atmosphere of a planet like Earth at a distance from its star that normalizes the wavelength integrated spectral constant to that of the Sun (1366 W/m^2) as a function of wavelength.

The wavelength of maximum photon flux (nm) is determined as,

$$\lambda_{\text{max, P}} = \frac{3.6697 \times 10^6}{T}$$

derived from the photon number flux peak, adjusted for Wien's law.

The photon flux at $\lambda_{\text{max, P}}$ (photons/m²/s/μm) is,

$$\Phi(\lambda_{\text{nm}}) = \frac{1.576 \times 10^{39}}{\lambda_{\text{nm}}^4} \frac{1}{e^{1.438776877 \times 10^7 / (\lambda_{\text{nm}} T)} - 1} \frac{1366}{\sigma T^4}$$

At $\lambda_{\text{nm}} = 3.6697 \times 10^6 / T$, $\Phi_{\text{max}} \approx 4.21 \times 10^{21} \text{ photons/m}^2/\text{s}/\mu\text{m}$.

In figure 7 the spectral photon flux $\Phi(\lambda_{\text{nm}})$ (photons/m²/s/μm) is plotted over the wavelength region 0–2000 nm for all star types. Identical photon flux at maximum across all star types is expected due to the normalization of integrated energy flux to 1366 W/m^2 . The scaling of $(R/d)^2 \propto 1/T^4$ and the photon flux's λ^{-4} dependence cancel out the temperature effects at the peak.

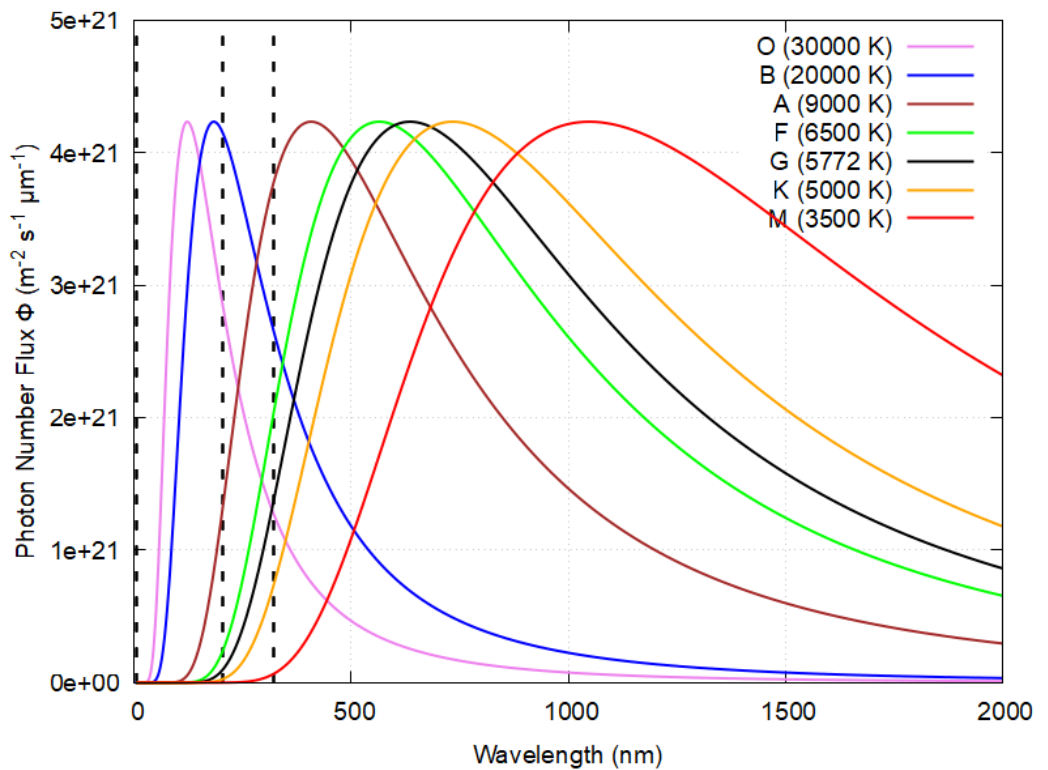


Figure 7. The photon fluxes of different star types at the top of the atmosphere of a planet like Earth as a function of wavelength at the distance of planet from star that normalizes the wavelength integrated spectral constant to that of the Sun (1366 W/m^2). The vertical dashed lines mark the wavelength limits of the hard (ionizing) UV-C radiation (10-205 nm) and soft (dissipative structuring) radiation (205-320 nm).

Figure 8 plots the ratio of the photon number fluxes as a function of wavelength for all star types compared to a G-type star, like our Sun, at the top of the atmosphere for a planet like Earth at the distance of planet from star that normalizes the wavelength integrated spectral constant to that of the Sun (1366 W/m^2).

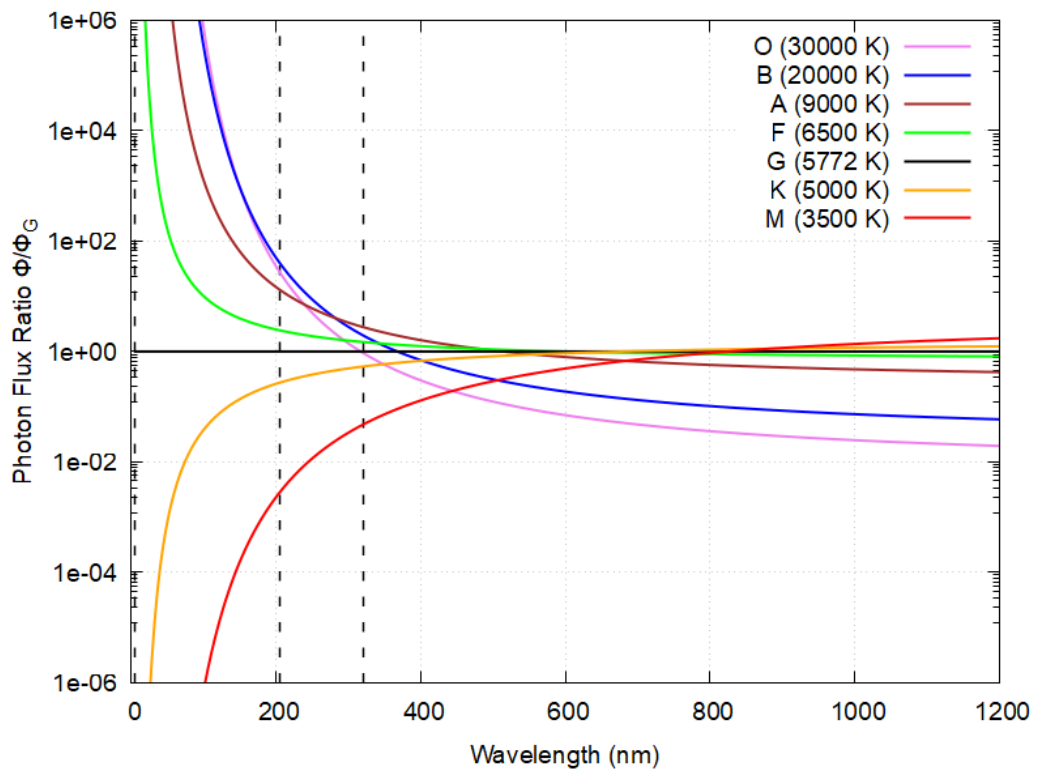


Figure 8. Ratio of photon number fluxes as a function of wavelength for all star types compared to a G type star, like our Sun, at the top of the atmosphere for a planet like Earth at the distance of planet from star that normalizes the wavelength integrated spectral constant to that of the Sun (1366 W/m^2). The vertical dashed lines mark the wavelength limits of the hard (ionizing) UV-C radiation (10–205 nm) and soft (dissipative structuring) radiation (205–320 nm).

7. Photon fluxes in Dissipative Structuring and Ionization Regions

For determining the viability of photon dissipative structuring on a given star type, spectral photon fluxes, rather than energy fluxes, are most relevant. Table 3 lists the integrated photon fluxes at the top of the planet's atmosphere with the planet–star distance normalized to give the same Earth–Sun solar constant. The spectral regions considered are; ionization/degradation, D (10–205 nm), dissipative production, P (205–320 nm) and HCN production, H (120–146 nm). The shortest wavelength of the destructive ionization region is taken to be 10 nm since there are few photons of shorter wavelength than this for all star types. The upper limit for the dissipative structuring regime is taken to be 320 nm corresponding to 3.9 eV since longer wavelengths do not have enough energy for transforming covalent bonds between organic elements.

HCN gas, an important precursor for the dissipative structuring of the nucleobases [15], can be produced in the upper atmosphere from the photon dissociation (120–146 nm) of N_2 and a carbon source (e.g., CH_4). The HCN gas produced would be protected in the lower atmosphere since the dissociation energy of the $\text{C}\equiv\text{N}$ triple bond of HCN is $\approx 744 \text{ kJ/mol}$ (7.71 eV or 161 nm).

Table 3. Total energy (W/m^2) and photon number fluxes ($\text{ph/m}^2/\text{s}$) at the top of the atmosphere of planets orbiting main-sequence stars at distances where the total energy flux at the top of the atmosphere equals the solar constant (1366 W/m^2). Wavelength ranges are D : 10–205 nm (ionization dissociation), P : 205–320 nm (dissipative production) and H : 120–146 nm (HCN production), and the Ratio P/D , based on integration of the photon fluxes under the curves of figure 7.

Star	T (K)	Total E Flux (W/m^2)	D ($\text{ph/m}^2/\text{s}$)	P ($\text{ph/m}^2/\text{s}$)	H ($\text{ph/m}^2/\text{s}$)	Ratio P/D
O7 V	30000	1366	6.107e20	2.677e20	1.288e20	0.438
B2 V	20000	1366	4.865e20	4.714e20	1.040e20	0.969
A2 V	9000	1366	5.321e19	3.660e20	3.558e18	6.880
F5 V	6500	1366	6.499e18	1.390e20	1.427e17	21.389
G2 V	5772	1366	2.319e18	8.165e19	2.998e16	35.203
K2 V	5000	1366	5.309e17	3.688e19	3.268e15	69.471
M2 V	3500	1366	3.550e15	2.142e18	1.945e12	603.459

Earth's early Archean atmosphere was described in section 2. Below 145 nm, N_2 absorbs strongly (peak at 98 nm), with CO_2 absorbing strongly between 120–170 nm (peak at 126 nm), and H_2S absorbing between 190–200 nm (peak at 195 nm). Aldehydes, such as formaldehyde, which are common photochemical products on a CO_2 atmosphere absorb strongly between 285–310 nm (roughly corresponding to the UV-B region). Modeling the absorption of these Archean atmospheric gases as Gaussians distributions centered on their peak absorption wavelength and with an extinction coefficient derived from their absorption cross section at maximum, the surface spectrum shown in figure 9 is obtained. Integration over the region 240–290 nm gives a surface energy flux of $\sim 5 \text{ W m}^{-2}$ for our Sun, which is consistent with estimates by Sagan [23].

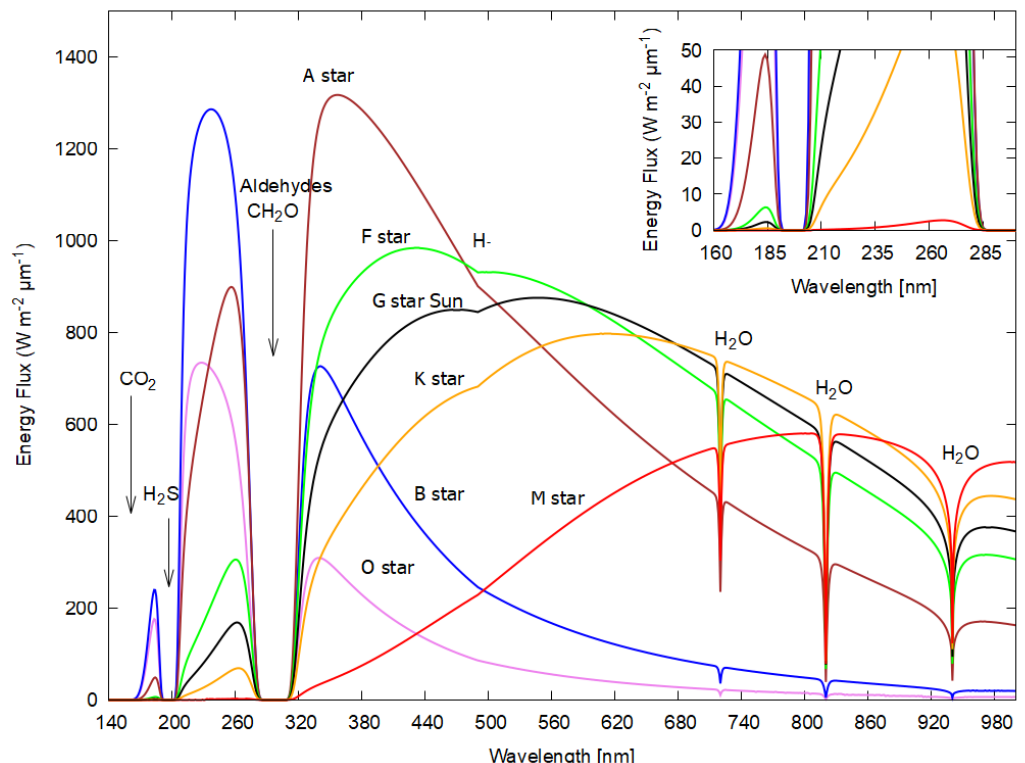


Figure 9. The energy fluxes of different star types at the surface of a planet like early Earth at a distance from its star that normalizes the wavelength integrated spectral constant to that of the Sun (1366 W/m^2) as a function of wavelength. The inset is an amplification of the UV-C region.

Table 4 lists the values of the total integrated energy flux at the surface as well as the number of photons in the degradation wavelength region D (10–205 nm), dissipative production region P (205–320 nm), and HCN production region H (120–146 nm), and the Ratio P/D . For the larger stars, with a greater proportion of energy emitted at short wavelength, most of the incident energy is absorbed in the atmosphere of the planet and does not reach the surface.

Table 4. Total energy (W/m^2) and photon number ($\text{ph}/\text{m}^2/\text{s}$) fluxes at the surface of a planet like Earth orbiting main-sequence stars at distances where the total energy flux at the top of the atmosphere equals the solar constant ($1366 \text{ W}/\text{m}^2$). Wavelength ranges are D : 10–205 nm (ionization destruction), P : 205–320 nm (dissipative production) and H : 120–146 nm (HCN production), and the Ratio P/D , based on integration of the photon fluxes under the curves of figure 9.

Star	T (K)	Total E Flux (W/m^2)	D ($\text{ph}/\text{m}^2/\text{s}$)	P ($\text{ph}/\text{m}^2/\text{s}$)	H ($\text{ph}/\text{m}^2/\text{s}$)	Ratio P/D
O7 V	30000	91.57	1.930e18	5.099e19	9.945e11	26.422
B2 V	20000	208.1	2.596e18	9.251e19	6.875e11	35.640
A2 V	9000	522.9	4.999e17	6.040e19	1.134e10	120.835
F5 V	6500	602.8	6.301e16	1.885e19	2.534e08	299.074
G2 V	5772	618.9	2.199e16	1.004e19	4.020e07	456.715
K2 V	5000	629.7	4.771e15	3.954e18	2.931e06	828.773
M2 V	3500	631.0	2.436e13	1.504e17	4.417e02	6173.985

8. Net Molecular Photochemical Production on Planets for Each Star Type

8.1. Rate equation

Photochemically dissipatively structured molecules not only have to survive dissociation or degradation by ionizing radiation, but also natural chemical destructive processes occurring at finite temperature in water solvent. For example, a study [58] on adenosine hydrolysis (glycosidic bond cleavage between adenine and ribose) at pH 7, extrapolated to 85°C (early Archean surface temperature [27,33,59]) via an Arrhenius plot from measurements at 110–190°C gives, $k = 1.038 \pm 0.360 \times 10^{-8} \text{ s}^{-1}$. This corresponds to a half-life of approximately 2.12 years (activation parameters $\Delta H^\ddagger = 28.0 \text{ kcal/mol}$ and $\Delta G^\ddagger = 32.9 \pm 0.3 \text{ kcal/mol}$). As another example, for adenine residues in DNA, deamination to hypoxanthine occurs at pH 7.6, 110 °C with a rate constant of $k = 4 \times 10^{-8} \text{ s}^{-1}$ [60].

Here we consider a photochemical dissipative structuring sequence requiring 6 independent photon absorption steps to produce the final molecule M (similar to the production of adenine [15]) starting with an initial constant concentration $[M_0]$ of the precursor (e.g., HCN). For each step, $M_{i-1} + \text{photon (flux } P\text{)} \rightarrow M_i$ with rate $\alpha P [M_{i-1}]$ (assuming the same rate constant α for all steps). For each intermediate molecule M_i ($i=1$ to 5) and final M ($i=6$), destruction by ionizing photon flux D with rate $\beta D [M_i]$ occurs as well as chemical destruction with rate constant k (e.g., hydrolysis or deamination), also assumed the same for all intermediates.

The differential equations describing the concentration dynamics are,

$$\begin{aligned}
\frac{d[M_1]}{dt} &= \alpha P[M_0] - (\alpha P + \beta D + k)[M_1], \\
\frac{d[M_2]}{dt} &= \alpha P[M_1] - (\alpha P + \beta D + k)[M_2], \\
&\vdots \\
\frac{d[M_5]}{dt} &= \alpha P[M_4] - (\alpha P + \beta D + k)[M_5], \\
\frac{d[M]}{dt} &= \alpha P[M_5] - (\beta D + k)[M].
\end{aligned} \tag{3}$$

The initial concentration for the precursor is taken to be $[M_0](0) = 6 \times 10^{-5}$ M (e.g., HCN, see ref. [15]), and the intermediates $[M_i](0) = 0$ for $i=1$ to 5.

Most hydrolysis rate constants at 85 °C for small molecules are between 1×10^{-7} s⁻¹ and 1×10^{-6} s⁻¹. For example, for HCN, formamide, and AICN (molecules on route to adenine) they are 5.13×10^{-7} , 6.69×10^{-7} and 2.94×10^{-7} respectively [15]. Any other chemical reactions will increase this rate of degradation. The nominal value of the chemical degradation rate constant k is therefore assigned to $k = 5 \times 10^{-7}$ s⁻¹ ($t_{1/2} \approx 160$ days) for each photochemical step, but results are also obtained for k an order of magnitude greater and lesser.

The rate constants for photochemical production α and destruction β are given by,

$$\alpha = q_P \cdot \sigma_P \text{ and } \beta = q_D \cdot \sigma_D$$

where q_P and q_D are the quantum efficiencies for the photochemical reaction, and σ_P and σ_D are the molecular photon absorption cross sections.

The photon absorption cross section σ (cm²/molecule) is related to the extinction coefficient ϵ (M⁻¹ cm⁻¹) by,

$$\sigma = \frac{\epsilon \cdot \ln(10)}{N_A \cdot 10^3} \tag{4}$$

where $N_A = 6.022 \times 10^{23}$ molecules/mol, $\ln(10) \approx 2.3026$, and 10^3 converts L to cm³.

For convenience, all 6 photochemical reactions are assumed to proceed at the same rate. However, in the case of the dissipative structuring of adenine, values of the quantum efficiencies q range from about 5×10^{-3} to 5×10^{-1} with the larger values associated to charge transfer reactions and smaller values associated to molecular transformations through high energy barriers. The extinction coefficients ϵ range from about 10^1 to 10^4 M⁻¹ cm⁻¹ (tables 1 and 2 of reference [15]). Therefore, for all 6 photochemical reactions we take values representative of intermediate molecular transformations on route to adenine of $q_P = 5 \times 10^{-2}$ and $\epsilon = 2,000$ M⁻¹ cm⁻¹ ($\sigma_P = 7.647 \times 10^{-24}$ cm²/molecule, Eq. 4). These values give,

$$\alpha = q_P \cdot \sigma_P = 3.8235 \times 10^{-25} \tag{5}$$

β is then determined as the value which gives the concentration at 30 Archean days $[M](30 \text{ days}) = 5 \times 10^{-8}$ M, which is what was found in a detailed calculation for the production of adenine including all relevant photochemical and chemical reactions (figures 10 and 11 of reference [15]). The rate constants for production and degradation obtained in this manner are therefore, $\alpha = 3.8235 \times 10^{-25}$ (s⁻¹) and $\beta = 1.6365 \times 10^{-22}$ (s⁻¹), respectively.

Equations (3) are solved numerically in time steps of one second using the values of photon fluxes P and D given in table 4 for each star type during the 3.5 hour daylight (sun at zenith) period, and $P = 0$ and $D = 0$ during the 10.5 hour night period of a 14 hour Archean day.

Figure 10 shows the time dependence of the molecular concentrations over 30 Archean days for the three different values of k for each star type. The graph shows a rapid rise

to low concentrations, on the order of 10^{-12} , 10^{-11} and 10^{-9} M for O, B and A-type stars respectively, and a slower rise to very low concentrations for M-type stars ($\sim 5 \times 10^{-18}$ M). Much higher concentrations ($\sim 10^{-7}$ M) are found for the G and F-type stars. The plots for the two smallest values of k almost overlap, indicating that at these k values chemical degradation has little effect on the concentrations.

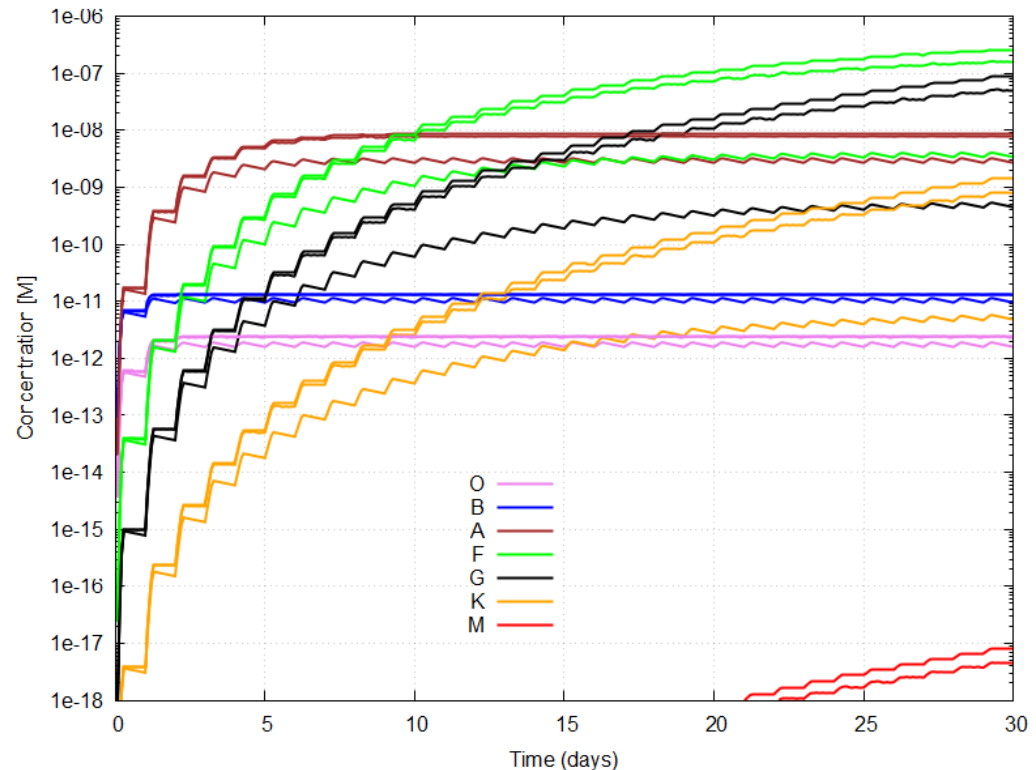


Figure 10. The concentration of a fundamental molecule requiring 6 independent photochemical reactions (e.g., adenine) as a function of time in Archean days (3.5 hours of light and 10.5 hours of darkness) on planets of different star types (different colors) at distances from their star normalized to the solar constant. The plots assume photochemical production (dissipative structuring, $\alpha = 3.8235 \times 10^{-25} \text{ m}^2/\text{photon}$) and photodegradation, $\beta = 1.6365 \times 10^{-22} \text{ m}^2/\text{photon}$). Results are plotted for three values of k , the nominal value of $5 \times 10^{-7} \text{ s}^{-1}$ (middle curve), $5 \times 10^{-8} \text{ s}^{-1}$ (upper curve) and $5 \times 10^{-6} \text{ s}^{-1}$ (lower curve).

Figure 11 plots the concentrations out to 300 days.

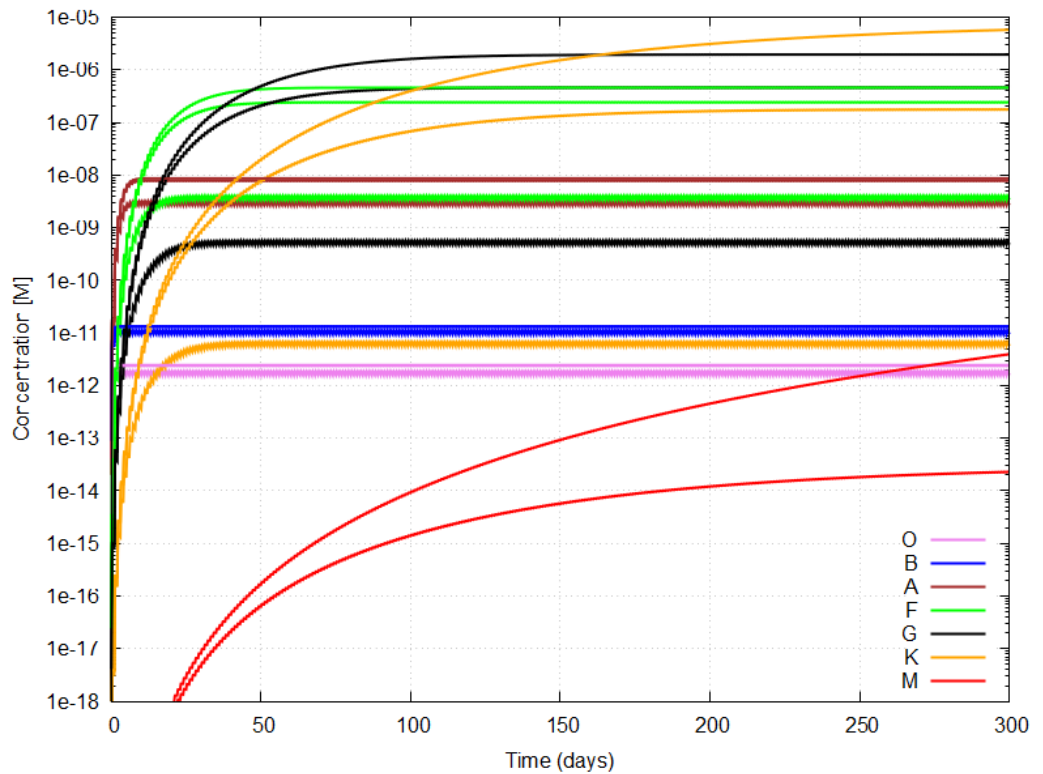


Figure 11. The same as for figure 10 but with the calculations extended out to 300 Archean days.

In the stationary (steady) state ($t \rightarrow \infty$), the concentrations are approximately,

$$[M]_{\infty} \approx [M_0] \left(\frac{0.25\alpha P}{0.25\alpha P + 0.25\beta D + k} \right)^5 \frac{0.25\alpha P}{(0.25\beta D + k)},$$

where the factor of $0.25 = 3.5/14$ accounts the 3.5 hours of direct overhead sunlight in a 14 hour Archean day.

The time to reach 99% of $[M]_{\infty}$ is approximated during the light period, where the system approaches $[M]_{\infty}$. The solution for $[M]$ is complicated due to the sequential reactions, but the rate-limiting step is governed by $\beta D + k$. Thus:

$$[M](t) \approx [M]_{\infty} \left(1 - e^{-(\beta D + k)t} \right), \quad (6)$$

and setting $[M](t) = 0.99[M]_{\infty}$ gives,

$$1 - e^{-(\beta D + k)t} \approx 0.99, \quad (7)$$

or,

$$t \approx \frac{\ln(100)}{\beta D + k} \approx \frac{4.60517}{\beta D + k}. \quad (8)$$

Since the light period is $3.5/14$ of the day (50400 s), the time in Archean days (t_d) to reach 99% of $[M]_{\infty}$ is,

$$t_d = \frac{14}{3.5 \cdot 50400} \cdot t \approx \frac{4.60517}{(\beta D + k) \cdot 12600}. \quad (9)$$

Table 5 lists the stationary state concentrations and the time to reach 99% of this value for each star type given the production P and degradation D photon fluxes and the three k values.

In figure 12 the stationary state values of the concentrations are plotted versus the time in days to reach 99% of the stationary state value for all star types and for the three k values.

Table 5. Stationary concentrations $[M]_\infty$ (mol/L) and time to 99% $[M]_\infty$ (Archean days) for planets on different star types, with $[M_0] = 6.0 \times 10^{-5}$ mol/L, $\alpha = 3.8235 \times 10^{-25}$ m²/photon, $\beta = 1.6365 \times 10^{-22}$ m²/photon, 14-hour Archean day (3.5 hours light, 10.5 hours dark), and for the three k (s⁻¹) values.

Star	P ph/m ² /s ¹	D ph/m ² /s ¹	$k = 5.0 \times 10^{-8}$		$k = 5.0 \times 10^{-7}$		$k = 5.0 \times 10^{-6}$	
			$[M]_\infty$ (M)	Time (days)	$[M]_\infty$ (M)	Time (days)	$[M]_\infty$ (M)	Time (days)
O7 V	5.099e19	1.930e18	2.451e-12	1.16	2.373e-12	1.16	1.732e-12	1.14
B2 V	9.251e19	2.596e18	1.337e-11	0.86	1.305e-11	0.86	1.035e-11	0.85
A2 V	6.040e19	4.999e17	8.655e-9	4.46	7.780e-9	4.44	2.941e-9	4.21
F5 V	1.885e19	6.301e16	4.581e-7	35.3	2.411e-7	33.8	3.732e-9	23.9
G2 V	1.004e19	2.199e16	1.945e-6	100	4.581e-7	89.2	5.233e-10	42.5
K2 V	3.954e18	4.771e15	7.592e-6	440	1.768e-7	285	6.262e-12	63.2
M2 V	1.504e17	2.436e13	8.700e-9	6770	2.908e-14	725	3.338e-20	73.0

values (hydrolysis or other chemically mediated degradation). For the nominal value of $k = 5 \times 10^{-7}$, G-type stars give the highest molecular concentrations (4.58×10^{-7} M), with smaller values for F and K-type stars (2.41×10^{-7} and 1.77×10^{-7} M, respectively).

For the nominal value of k , the time to reach these stationary values is 34, 89 and 285 Archean days for F, G and K-types, respectively (see table 5 and figure 12). O and B stars produce stationary concentrations about 5 orders of magnitude smaller than G-type stars, while M stars produce stationary concentrations 7 orders of magnitude smaller, and it takes much longer (725 Archean days) to reach this very low stationary concentration.

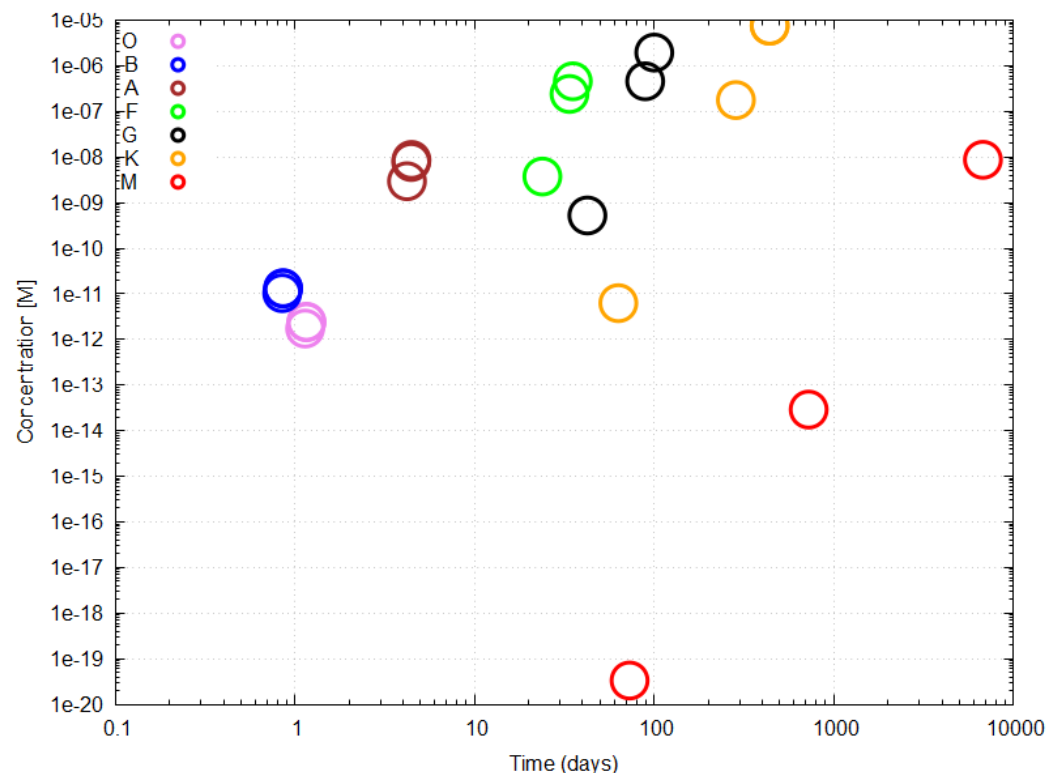


Figure 12. Stationary state values of the concentrations versus the time in days to reach 99% of this value for each star type and for the three chemical degradation rate constants k , of 5×10^{-8} , 5×10^{-7} and 5×10^{-6} (giving highest to lowest stationary state concentrations, respectively). For O and B-type stars, all three k values give similar results, indicating that chemical degradation has little effect on these molecular concentrations. Both axis are logarithmic.

Stationary state concentrations are important when predicting the probability of photon dissipative structuring of life like our own on planets of other star types. Very low concentrations will inhibit the formation of polymers like RNA, DNA or proteins. The time to reach such concentrations is also important because periodic catastrophic events, like meteor impacts or stellar outbursts, could reset concentrations. Catastrophic events and their frequency of occurrence, as well as other factors affecting molecular buildup, are considered in the following subsection.

8.2. Other Factors Important to Molecular Buildup

8.2.1. Precursor Concentrations

The above calculations were modeled on the dissipative structuring of adenine, treated in detail elsewhere [15]. For adenine and the other nucleobases, as well as for important amino acids, it is generally assumed that HCN or its derivatives were the precursors.

HCN stationary state concentrations were assumed to be the same and constant (5×10^{-6} M [15]) for all planets on the different star types. Most of the HCN production on early Earth was through photochemical reactions in Earth's upper atmosphere [15]. Since the integrated photon flux in this HCN production region H (120–146 nm) for O and B-type stars have intensities 4 orders of magnitude greater than G-type stars, while M-type stars have intensities 4 orders of magnitude lower (table 3), it can be assumed that initial precursor concentrations will be different for planets on different star types.

The relation between photon flux and primordial HCN concentration in the sea surface microlayer is, however, nontrivial. Much will depend on the other competing UV-induced atmospheric photochemical reactions, which, as far as the authors are aware, have not been studied in detail for the spectra of massive stars. For example, the dissociation energy of HCN corresponds to a photon wavelength of approximately 93 nm, exactly where O-type stars peak in photon intensity.

What can be confidently stated, however, is that HCN concentrations in the planet sea surface microlayer for the less massive K and M-type stars will be lower, and therefore stationary concentrations of the fundamental molecules will be even lower than those determined here.

8.2.2. X-ray and Far-Ultraviolet Outbursts of Main-Sequence Stars

The average frequency of large ($>10^{32}$ erg) and small ($10^{30} - 10^{31}$ erg) X-ray (0.12–50 keV) or far-ultraviolet (FUV, 91–200 nm) outbursts is listed in table 6 for main-sequence stars G2V, K2V, and M2V, representing field stars ($\sim 1 - 5$ Gyr). Large flares increase the flux by factors of $\sim 10 - 100$, while small flares by factors of $\sim 2 - 10$, lasting minutes to hours.

Table 6. Frequency of large ($>10^{32}$ erg) and small ($10^{30} - 10^{31}$ erg) X-ray (0.12–50 keV) or far-ultraviolet (FUV, 91–200 nm) X-ray and FUV outbursts for main sequence G2V, K2V, and M2V stars. Frequencies are the mean time in days between flares, derived from ROSAT, XMM-Newton, and GALEX data, with ranges reflecting variability in rotation and magnetic activity. Frequencies are higher for younger stars ($\sim 10 - 625$ Myr) and lower for older stars (>5 Gyr).

Star Type	Frequency of Large Outbursts (days)	Frequency of Small Outbursts (days)
G2V	365–3650	0.2–2
K2V	7–30	0.2–1
M2V	3–30	0.05–0.2

Without oxygen or ozone, the Archean atmospheres would allow $\sim 4\%$ of incident X-ray or FUV flares to reconstitute as hard ionizing UV-C (10–205 nm) radiation at the surface. This could inhibit the buildup of the fundamental molecules and is particularly relevant

for M-type stars where stationary state concentrations take many months to develop and are very low (see table 5).

Outbursts on more massive stars are much less frequent and of lower intensity due to the convection cells at deeper stellar depth and the distance of the planets from their stars.

8.2.3. Energetic Stellar Particle Winds

Low mass stars, where convection cells reach closer to the surface, besides being prone to X-ray and FUV outbursts, also produce energetic ionized particle winds which could deplete planetary atmospheres [61] and, in particular, O₃ columns [62,63]. This again would be problematic for life on planets of M and K-type stars that had survived earlier evolution and was developing oxygenic photosynthesis through more complex and more hard UV-C vulnerable biosynthetic pathways.

8.2.4. Stellar Lifetimes

The more massive a star, the higher its internal temperature and therefore the greater its rate of nuclear burning, implying shorter lifetimes (Table 7).

Table 7. Average lifetimes in Gyr (10⁹ years) for representative spectral types of main-sequence stars. Lifetimes are derived from stellar evolution models with lifetimes scaling approximately as $\tau \propto M^{-2.5}$, M being the stellar mass in solar masses. Ranges account for variations in mass and metallicity [64–67].

Spectral Type	Lifetime (Gyr)
O5V	0.001–0.003
O9V	0.003–0.005
B0V	0.01–0.02
B5V	0.05–0.1
A0V	0.4–0.6
A5V	0.8–1.0
F0V	1.5–2.0
F5V	2.5–3.5
G0V	8–10
G2V	10
G5V	10–12
K0V	15–20
K2V	20–30
K5V	30–50
M0V	50–70
M2V	70–100
M5V	100–200

The earliest widely accepted evidence for bacteria on Earth date from about 3.45 Ga [68], or about 1 Gyr after our Sun arrived on the main sequence. Assuming such a time scale to be representative of carbon based life, table 7 suggests that, besides the low concentrations of fundamental molecules, because of evolutionary times required, it would be highly improbable to find biosignatures of such developed life on O, B and the larger A-type stars.

8.2.5. Tidal Locking

The dissipation of a planet's rotational energy through gravitational interaction with its star (and moons), implies that planets in habitable zones located particularly close to their stars may become tidally locked, leaving one side in eternal starlight and the other in eternal darkness.

For the dissipative structuring of chromophores, like the fundamental molecules of life, this is not necessarily an impediment. However, the TDTOL also argues that more complex

biosynthetic structuring during the Archean was dependent on the diurnal cycle of sunlight [2]. For example, the enzyme-less denaturing and extension of RNA and DNA, and, as a consequence, life's homochirality, are predicted by TDTOL to require diurnal cycling of the UV-C light and high ocean surface temperatures (Ultraviolet and Temperature Assisted Replication - UVTAR [11,13]). Planets on M and lower mass K-type stars in their habitable zone may become tidally locked within a few hundred million years, thereby arresting continued evolution beyond the UV-C pigment epoch of dissipatively structured carbon based life.

9. Relevant Biosignatures Under TDTOL

If TDTOL is indeed the correct theory describing abiogenesis of carbon based life on Earth, a natural biosignature to consider would be the global planetary photon dissipation rate. According to the theory, photon dissipation begins in the soft UV-C region and gradually evolves pigments to dissipate longer wavelengths. The more developed the biosphere (i.e., with greater biomass and thermodynamic coupling of organisms at different hierachal levels and with abiotic dissipative processes), the greater the global photon dissipation or entropy production. Such a biosignature would entail measuring the planet's incident and emitted spectra and then accurately determining the entropy production based on the Planck radiation formula, as detailed in references [3,16].

Emitted spectra of extrasolar planets are presently difficult to measure due to the saturating light of the star, especially for the intermediate mass stars for which TDTOL predicts the most probable occurrence of molecular dissipative structuring. A less challenging proxy measurement, therefore, may be the soft UV-C planet albedo. According to TDTOL, this should be low after the formation of a primordial UV-C pigment world [20], and would remain low throughout biotic evolution of the planet.

Figure 13 presents the simulated wavelength dependent albedo of present day Earth. The albedo at soft UV-C wavelengths is very low, attributed to the ozone and oxygen in the stratosphere (~ 30 km altitude), which, as we have proposed in a previous publication [8], can be considered as life-derived pigments.

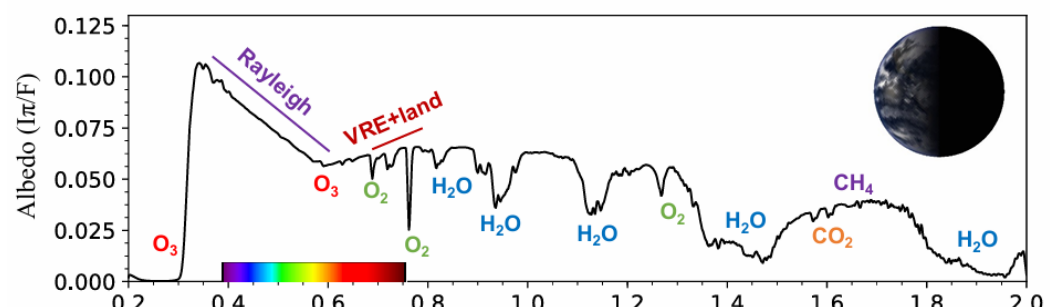


Figure 13. The simulated wavelength dependent albedo of present day Earth [69] as a function of wavelength (μm). The soft UV-C albedo (205–285 nm) is very low, due principally to the absorption by ozone, which is considered within TDTOL to be a life produced UV-C pigment. It is argued that this region of the spectrum would have low albedo at the beginning of life, and would remain low throughout the entire evolution of life and, therefore, may be a more easily measured biosignature for carbon based life on a planet at all stages of its evolution. Saturation effects due to Rayleigh scattering off atmospheric molecules with a $1/\lambda^4$ dependence is noted on the plot and would have to be accounted for in the soft UV-C region for planets with early life which had not yet reached the stage of oxygenic photosynthesis. The inset depicts the Earth at half illumination for which the simulation was performed. Reprinted from Schwieterman et al. [69,70] under Creative Commons Attribution License CC-BY.

During the Archean without oxygen or ozone, this light would have made it to the Earth's surface (figure 1) where it would have been absorbed by the fundamental molecules

of life (UV-C pigments) giving, again, relatively low albedo. Rayleigh scattering (see figure 13) on the atmosphere will dilute this albedo signal somewhat, but could be corrected for once the densities of the relevant atmospheric gases were determined.

10. Discussion

Under the postulates of the Thermodynamic Dissipation Theory of the Origin of Life (TDTOL) which describes photochemical molecular dissipative structuring, we have analyzed the suitability of star types for the abiogenesis of life similar to ours, on a planet similar to early Earth, at a distance from their star normalizing the stellar constant to the solar constant.

O type stars have high photon fluxes in the ionization region (< 205 nm) leading to very low molecular steady state concentrations (on the order of 10^{-5} that of G-type stars). Furthermore, the dissociation energy of one of the most important precursors for Earth's fundamental molecules, HCN, corresponds to a photon wavelength of approximately 93 nm, exactly where O-type stars peak in photon intensity, implying little probability of this important precursor raining down to the surface on such a planet. These stars also have very short lifetimes, < 0.005 Ga, implying improbable evolution to complex lifeforms such as bacteria, which took roughly 0.35 Ga on Earth.

B-type stars suffer from the same afflictions as O-type stars, but to a somewhat lesser degree. For example, their dissipatively structured stationary state molecular concentrations for a nominal hydrolysis rate constant ($k = 5 \times 10^{-7} \text{ s}^{-1}$) are more than four orders of magnitude smaller than that predicted for G type stars (Table 5). Their maximum lifetimes of ~ 0.1 Gyr again suggests low probability of finding bacteria on their planet surfaces.

The less massive A-type stars have stationary state molecular concentrations about two orders of magnitude lower than that of G-type stars and may live long enough ~ 1 Gyr for the evolution to bacteria, but the greater than one order of magnitude higher hard UV-C (< 205 nm) radiation (see Table 5, column D) could cause other problems for incipient life not considered here, for example, greater production of free radicals in water, requiring a thicker atmosphere than Earth's Archean to filter out the harmful hard UV-C light.

F and G-type stars appear to be the most adequate for the appearance of life like our own through photochemical molecular dissipative structuring. They would have high stationary state concentrations of the fundamental molecules and arrive at these stationary state values within short time periods (a few months). They have low rates of X-ray, FUV or particle outbursts and they live long enough for the evolution of bacteria and even complex ecosystems. However, shorter stellar lifetimes of F type stars (~ 2 Ga) imply that intelligent human-like civilizations probably only arise on G-type stars. F and G-type stars sum to only about 8-10% of all stars in our galaxy [64].

K-type stars suffer from a number of impediments to the dissipative structuring of life on their planets within habitable zones. First, although their the stationary state concentrations of the fundamental molecules are similar to that of G-type stars, they are more prone to natural periodic catastrophic events. Frequent outbursts of high intensity short wavelength FUV, X-rays and high energy particles with average periods of only days could degrade chromophores formed in the soft UV-C. An order of magnitude of lower intensity of the HCN production region H of the spectrum (Table 3) would result in a similar decrease in the fundamental molecule concentrations. Tidal locking of planets on lower mass K-type stars would also mean that diurnal cycling, necessary for UV-C induced denaturing [13] and homochirality [11] as well as night time extension (enzyme-less RNA/DNA replication) and thus subsequent evolution under TDTOL, would not occur. These impediments, however, may be less critical for high mass K-type stars.

M-type stars will have very low stationary concentrations of the fundamental molecules, less than 10^{-7} that of G-type stars for nominal $k = 5 \times 10^{-7} \text{ s}^{-1}$ (table 5 and figure 12). A four orders of magnitude lower intensity in the HCN production region H of the spectrum (table 3) would mean a similar decrease in the fundamental molecule concentrations, bringing fundamental molecule concentrations to only perhaps 10^{-11} that of G-type stars.

Furthermore, they require very long times (years) to reach even these very low concentrations and are subjected to very frequent outbursts of high intensity short wavelength FUV, X-rays and high energy particles which would degrade any viable molecules. Their planets in the habitable zone will also become tidally locked, negating evolution through diurnal effects.

Our analysis for the development of life according to the molecular dissipative structuring theory of abiogenesis as detailed in the TDTOL, assumed an Earth-like planet with a primordial atmosphere similar to the present best determinations of Earth's early Archean. The affect of a thicker or thinner atmosphere on reducing or increasing the photon fluxes at the planetary surface would have to be modeled and the relevant table of surface photon fluxes, table 4, determined. The same would also be required for larger or smaller planets than Earth because, in general, larger or smaller planets will support denser or thinner atmospheres, respectively.

The greater the number of photochemical steps n required in the production of a given fundamental molecule, the greater the dependency of the stationary concentrations on both the ratios of the photon fluxes P/D and the quantum efficiencies α/β , as, for example, indicated by the dependence of the stationary state concentrations on these,

$$[M]_{\infty} \approx [M_0] \left(\frac{0.2857\alpha P}{0.2857\alpha P + 0.2857\beta D + k} \right)^{n-1} \frac{0.2857\alpha P}{(0.2857\beta D + k)}.$$

For example, for the nominal value of $k = 5 \times 10^{-7}$, in going from $n = 6$ to $n = 8$ the ratio of stationary concentrations of the fundamental molecules for G-type stars over that for M-type stars goes from 10^7 to 10^9 . The more photons involved in the dissipative structuring, the less likely the molecule will be found on lower mass M or K-type stars and the greater the probability of finding them on higher mass stars.

Our analysis assumed black-body spectra which tend to overestimate the true intensity of UV-C wavelengths due to stellar atmosphere absorption lines. However, these absorption lines would be relatively similar for all star types since they are attributed to the common ionized elements and molecules like CO, CN, and OH.

11. Conclusion

Given our analysis under the postulates of the TDTOL, and given the known physical parameters of star types, we conclude that astrobiologists should concentrate their searches for bacterial biosignatures only on F, G and higher mass K-type stars, and biosignatures of intelligent life only on G and high mass K-type stars. Under TDTOL, is highly unlikely that life, as we know it, would be found on M-type stars, unless some kind of panspermia from an F or G-type star had occurred once visible photosynthesis had arisen on planets of these stars. Possibilities may include binary star systems with one component being an F or G-type star and the other an M-type star.

We have suggested a biosignature involving the global planetary entropy production for which the incident and emitted planet spectra would need to be measured. The difficulty associated with making spectroscopic observations of planetary atmospheres on F and G type stars, due to their high luminosities, could be avoided by considering instead a simpler proxy biosignature; the planetary soft UV-C (205–285 nm) albedo. A low value for this biosignature may indicate the possible existence of carbon based life, once corrected for Rayleigh scattering off atmospheric gases.

Our hope is that this work may help the astrobiology community select more appropriate star types for searching for carbon based life and guide them in developing the instruments and techniques needed for biosignature detection based on the fundamental thermodynamic function of life; that of photon dissipation (entropy production).

Funding: This research was funded by DGAPA-UNAM, grant number IN104920.

The following abbreviations are used in this manuscript:

CO ₂	carbon dioxide
DNA	deoxyribonucleic acid
FUV	Far Ultraviolet - light within the region 100-200 nm
hard UV-C	light in the region 100-205 nm
HCN	hydrogen cyanide
H ₂ S	hydrogen sulfide
RNA	ribonucleic acid
soft UV-C	light within the region 205-285 nm
TDTOL	Thermodynamic Dissipation Theory for the Origin of Life
UV-A	light within the region 315-400 nm
UV-B	light within the region 280-315 nm
UV-C	light within the region 100-280 nm
UVTAR	Ultraviolet and Temperature Assisted Replication

References

1. Michaelian, K. Thermodynamic origin of life. *ArXiv* **2009**, [arXiv:physics.gen-ph/0907.0042].
2. Michaelian, K. Thermodynamic dissipation theory for the origin of life. *Earth Syst. Dynam.* **2011**, 224, 37–51, [<https://esd.copernicus.org/articles/2/37/2011/esd-2-37-2011.html>]. <https://doi.org/10.5194/esd-2-37-2011>.
3. Michaelian, K. The Biosphere; INTECH: London, 2012; chapter The biosphere: A thermodynamic imperative, pp. 51–60.
4. Michaelian, K. Biological catalysis of the hydrological cycle: life's thermodynamic function. *Hydrol. Earth Syst. Sci.* **2012**, 16, 2629–2645, [www.hydrol-earth-syst-sci.net/16/2629/2012/]. <https://doi.org/10.5194/hess-16-2629-2012>.
5. Michaelian, K. A non-linear irreversible thermodynamic perspective on organic pigment proliferation and biological evolution. *Journal of Physics* **2013**, Conference Series 475, 012010, [<https://iopscience.iop.org/article/10.1088/1742-6596/475/1/012010/meta>].
6. Michaelian, K.; Santillán Padilla, N. DNA Denaturing through Photon Dissipation: A Possible Route to Archean Non-enzymatic Replication. *bioRxiv* **2014**, [<https://www.biorxiv.org/content/early/2014/09/12/009126>]. <https://doi.org/10.1101/009126>.
7. Michaelian, K.; Simeonov, A. Fundamental molecules of life are pigments which arose and co-evolved as a response to the thermodynamic imperative of dissipating the prevailing solar spectrum. *Biogeosciences* **2015**, 12, 4913–4937, [<https://bg.copernicus.org/articles/12/4913/2015/>].
8. Michaelian, K. *Thermodynamic Dissipation Theory of the Origin and Evolution of Life: Salient characteristics of RNA and DNA and other fundamental molecules suggest an origin of life driven by UV-C light*; Self-published. Printed by CreateSpace. Mexico City. ISBN:9781541317482., 2016.
9. Michaelian, K. Microscopic Dissipative Structuring and Proliferation at the Origin of Life. *Heliyon* **2017**, 3, e00424, [<https://www.ncbi.nlm.nih.gov/pmc/articles/PMC5647473/>]. <https://doi.org/10.1016/j.heliyon.2017.e00424>.
10. Michaelian, K.; Simeonov, A. Thermodynamic explanation of the cosmic ubiquity of organic pigments. *Astrobiol. Outreach* **2017**, 5, 156, [<https://www.longdom.org/open-access/thermodynamic-explanation-for-the-cosmic-ubiquity-of-organicpigments-2332-2519-1000156.pdf>].
11. Michaelian, K. Homochirality through Photon-Induced Denaturing of RNA/DNA at the Origin of Life. *Life* **2018**, 8, [<http://www.mdpi.com/2075-1729/8/2/21>]. <https://doi.org/10.3390/life8020021>.
12. Michaelian, K.; Rodriguez, O. Prebiotic fatty acid vesicles through photochemical dissipative structuring. *Revista Cubana de Química* **2019**, 31, 354–370.
13. Michaelian, K.; Santillan, N. UVC photon-induced denaturing of DNA: A possible dissipative route to Archean enzyme-less replication. *Heliyon* **2019**, 5, e01902, [<https://www.heliyon.com/article/e01902>].
14. Michaelian, K. Photochemical Dissipative Structuring of the Fundamental Molecules of Life. *Proceedings, 5th International Electronic Conference on Entropy and Its Applications; Session: Biological Systems* **2019**.
15. Michaelian, K. The Dissipative Photochemical Origin of Life: UVC Abiogenesis of Adenine. *Entropy* **2021**, 23, [<https://www.mdpi.com/1099-4300/23/2/217>]. <https://doi.org/10.3390/e23020217>.

16. Michaelian, K.; Cano, R.E. A Photon Force and Flow for Dissipative Structuring: Application to Pigments, Plants and Ecosystems. *Entropy* **2022**, *24*, 76. <https://doi.org/10.3390/e24010076>.
17. Michaelian, K. Non-Equilibrium Thermodynamic Foundations of the Origin of Life. *Foundations* **2022**, *2*, 308–337. <https://doi.org/10.3390-foundations2010022>.
18. Hernández, C.; Michaelian, K. Dissipative Photochemical Abiogenesis of the Purines. *Entropy* **2022**, *24*, 1027. <https://doi.org/10.3390/e24081027>.
19. Michaelian, K. The Non-Equilibrium Thermodynamics of Natural Selection: From Molecules to the Biosphere. *Entropy* **2023**, *25*. <https://doi.org/10.3390/e25071059>.
20. Michaelian, K. The Pigment World: Life's Origins as Photon-Dissipating Pigments. *Life* **2024**, *14*. <https://doi.org/10.3390/life14070912>.
21. Ferris, J.P.; Orgel, L.E. An Unusual Photochemical Rearrangement in the Synthesis of Adenine from Hydrogen Cyanide. *J. Am. Chem. Soc.* **1966**, *88*, 1074–1074.
22. Barks, H.L.; Buckley, R.; Grieves, G.A.; Di Mauro, E.; Hud, N.V.; Orlando, T.M. Guanine, Adenine, and Hypoxanthine Production in UV-Irradiated Formamide Solutions: Relaxation of the Requirements for Prebiotic Purine Nucleobase Formation. *ChemBioChem* **2010**, *11*, 1240–1243, [https://chemistry-europe.onlinelibrary.wiley.com/doi/pdf/10.1002/cbic.201000074]. <https://doi.org/10.1002/cbic.201000074>.
23. Sagan, C. Ultraviolet Selection Pressure on the Earliest Organisms. *J. Theor. Biol.* **1973**, *39*, 195–200.
24. Mulkidjanian, A.Y.; Cherepanov, D.A.; Galperin, M.Y. Survival of the fittest before the beginning of life: selection of the first oligonucleotide-like polymers by UV light. *BMC Evolutionary Biology* **2003**, *3*, 12. <https://doi.org/10.1186/1471-2148-3-12>.
25. Powner, M.; Gerland, B.; Sutherland, J. Synthesis of activated pyrimidine ribonucleotides in prebiotically plausible conditions. *Nature* **2009**, *459*, 239–242.
26. Kufner, C.L.; Bucher, D.B.; Sasselov, D.D. The Photophysics of Nucleic Acids: Consequences for the Emergence of Life. *ChemSystemsChem* **2023**, *5*, e202200019. <https://doi.org/10.1002/syst.202200019>.
27. Kasting, J. Earth's Early Atmosphere. *Science* **1993**, *259*, 920–926.
28. Lowe, D.R.; Tice, M.M. Geologic evidence for Archean atmospheric and climatic evolution: Fluctuating levels of CO₂, CH₄, and O₂ with an overriding tectonic control. *Geology* **2004**, *32*, 493–496.
29. Catling, D.C.; Zahnle, K.J. The Archean atmosphere. *Science Advances* **2020**, *6*, eaax1420. <https://doi.org/10.1126/sciadv.aax1420>.
30. Spalding, C.; Fischer, W.W. A shorter Archean day-length biases interpretations of the early Earth's climate. *Earth and Planetary Science Letters* **2019**, *520*, 155–164. <https://doi.org/10.1016/j.epsl.2019.05.015>.
31. Schwartz, A.W.; Chang, S. From Big Bang to Primordial Planet-Setting the Stage for the Origin of Life. In *Life's Origin*; Schopf, J.W., Ed.; University of California Press: Berkeley, 2002; pp. 78–112.
32. Knauth, L.P., Lecture Notes in Earth Sciences #43; Springer-Verlag, Berlin, 1992; chapter Isotopic Signatures and Sedimentary Records, pp. 123–152.
33. Knauth, L.P.; Lowe, D.R. High Archean climatic temperature inferred from oxygen isotope geochemistry of cherts in the 3.5 Ga Swaziland group, South Africa. *Geol. Soc. Am. Bull.* **2003**, *115*, 566–580.
34. Pflüger, E. Beitrag zur Lehre von der Respiration. I. Ueber die physiologische Verbrennung in den lebendigen organismen. *Arch. Ges. Physiol.* **1875**, *10*, 641–644.
35. Rimmer, P.B.; Rugheimer, S. Hydrogen cyanide in nitrogen-rich atmospheres of rocky exoplanets. *Icarus* **2019**, *329*, 124–137. <https://doi.org/10.1016/j.icarus.2018.12.011>.
36. Glansdorff, P.; Prigogine, I. *Thermodynamic Theory of Structure, Stability and Fluctuations*; Wiley - Interscience: Hoboken, NJ, USA, 1971.
37. Cnossen, I.; Sanz-Forcada, J.; Favata, F. and Witasse, O.; Zegers, T.; Arnold, N.F. The habitat of early life: Solar X-ray and UV radiation at Earth's surface 4–3.5 billion years ago. *J. Geophys. Res.* **2007**, *112*, E02008. <https://doi.org/10.1029/2006JE002784>.
38. Lechuga, I.; Michaelian, K. Fatty Acid Vesicles as Hard UV-C Shields for Early Life. *Foundations* **2023**, *3*, 99–114. <https://doi.org/10.3390-foundations3010010>.
39. Miller, S.L.; Orgel, L. The origins of life on the earth; Prentice-Hall, Englewood Cliffs, N.J., 1974.
40. Schurman, M.S.; Stolow, A. Dynamics at Conical Intersections. *Annu. Rev. Phys. Chem.* **2018**, *69*, 427–450.

41. Cohen, B.; Hare, P.M.; Kohler, B. Ultrafast Excited-State Dynamics of Adenine and Monomethylated Adenines in Solution: Implications for the Nonradiative Decay Mechanism. *Journal of the American Chemical Society* **2003**, *125*, 13594–13601, [<https://doi.org/10.1021/ja035628z>]. PMID: 14583057, <https://doi.org/10.1021/ja035628z>.
42. Sagan, C.; Khare, B.N. Long-Wavelength Ultraviolet Photoproduction of Amino Acids on the Primitive Earth. *Science* **1971**, *173*, 417–420, [<https://science.sciencemag.org/content/173/3995/417.full.pdf> <https://doi.org/10.1126/science.173.3995.417>].
43. Ruiz-Bermejo, M.; Zorzano, M.P.; Osuna-Esteban, S. Simple Organics and Biomonomers Identified in HCN Polymers: An Overview. *Life* **2013**, *3*, 421–448. <https://doi.org/10.3390/life3030421>.
44. Meinert, C.; Myrgorodska, I.; de Marcellus, P.; Buhse, T.; Nahon, L.; Hoffmann, S.V.; Le Sergeant d'Hendecourt, L.; Meierhenrich, U.J. Ribose and related sugars from ultraviolet irradiation of interstellar ice analogs. *Science* **2016**, *352*, 208–212. <https://doi.org/10.1126/science.aad8137>.
45. Michaelian, K.; Simeonov, A. The Dissipative Photochemical Origin of Photosynthesis. *in process* **2025**.
46. Meixnerová, J.; Blum, J.D.; Johnson, M.W.; Stüeken, E.E.; Kipp, M.A.; Anbar, A.D.; Buick, R. Mercury abundance and isotopic composition indicate subaerial volcanism prior to the end-Archean “whiff” of oxygen. *Proceedings of the National Academy of Sciences* **2021**, *118*, e2107511118, [<https://www.pnas.org/doi/pdf/10.1073/pnas.2107511118>]. <https://doi.org/10.1073/pnas.2107511118>.
47. Meller, R.; Moortgat, G.K. Temperature dependence of the absorption cross sections of formaldehyde between 223 and 323 K in the wavelength range 225–375 nm. *Journal of Geophysical Research: Atmospheres* **2000**, *105*, 7089–7101, [<https://agupubs.onlinelibrary.wiley.com/doi/pdf/10.1029/1999JD901074>]. <https://doi.org/https://doi.org/10.1029/1999JD901074>.
48. Orr-Ewing, A. Reaction Dynamics –Relaxation Pathways. *Lecture Notes; University of Bristol: Bristol, UK* **2014**, pp. 1–36.
49. Roberts, G.M.; Marroux, H.J.B.; Grubb, M.P.; Ashfold, M.N.R.; Orr-Ewing, A.J. On the Participation of Photoinduced N–H Bond Fission in Aqueous Adenine at 266 and 220 nm: A Combined Ultrafast Transient Electronic and Vibrational Absorption Spectroscopy Study. *The Journal of Physical Chemistry A* **2014**, *118*, 11211–11225, [<https://doi.org/10.1021/jp508501w>]. PMID: 25296392, <https://doi.org/10.1021/jp508501w>.
50. Kleinermanns, K.; Nachtigallová, D.; de Vries, M.S. Excited state dynamics of DNA bases. *International Reviews in Physical Chemistry* **2013**, *32*, 308–342, [<https://doi.org/10.1080/0144235X.2012.760884>]. <https://doi.org/10.1080/0144235X.2012.760884>.
51. Barbatti, M.; Aquino, A.; Szymczak, J.; Nachtigallová, D.; Hobza, P.; Lischka, H. Relaxation mechanisms of UV-photoexcited DNA and RNA nucleobases. *Proc Natl Acad Sci U S A* **2010**, *107*, 21453–21458. <https://doi.org/doi:10.1073/pnas.1014982107>.
52. Boulanger, E.; Anoop, A.; Nachtigalova, D.; Thiel, W.; Barbatti, M. Photochemical Steps in the Prebiotic Synthesis of Purine Precursors from HCN. *Angew. Chem. Int.* **2013**, *52*, 8000–8003.
53. Cauët, E.; Deharenq, D.; Liévin, J. Ab Initio Study of the Ionization of the DNA Bases in Water: Role of the First Hydration Shell. *ChemPhysChem* **2007**, *8*, 2112–2120. <https://doi.org/10.1002/cphc.200700334>.
54. Schroeder, C.A.; Pluhařová, E.; Seidel, R.; Schroeder, W.P.; Faubel, M.; Slavíček, P.; Winter, B.; Jungwirth, P.; Bradforth, S.E. Exploring Redox Properties of Aromatic Amino Acids in Water: Contrasting Single Photon vs Resonant Multiphoton Ionization in Aqueous Solutions. *Journal of the American Chemical Society* **2015**, *137*, 201–209. <https://doi.org/10.1021/ja508053m>.
55. Kumari, K.; Vaval, N. Ionization potential of small polyalcohols in gas phase and water medium: A theoretical study. *Chemical Physics Letters* **2013**, *573*, 44–49. <https://doi.org/10.1016/j.cplett.2013.04.032>.
56. Bravaya, K.B.; Kostko, O.; Dolgikh, S.; Landau, A.; Ahmed, M.; Krylov, A.I. Electronic structure and spectroscopy of nucleic acid bases: Ionization energies, ionization-induced structural changes, and photoelectron spectra. *The Journal of Physical Chemistry A* **2010**, *114*, 12305–12317. <https://doi.org/10.1021/jp1063726>.
57. Pecaut, M.J.; Mamajek, E.E. Intrinsic Colors, Temperatures, and Bolometric Corrections of Pre-main-sequence Stars. *The Astrophysical Journal Supplement Series* **2013**, *208*, 9. <https://doi.org/10.1088/0067-0049/208/1/9>.
58. Borquez, E.; Cleaves, H.; Lazcano, A.; Miller, S. An Investigation of Prebiotic Purine Synthesis from the Hydrolysis of HCN Polymers. *Orig Life Evol Biosph* **2005**, *35*, 79–90.

59. Kasting, J.F.; Ackerman, T.P. Climatic consequences of very high carbon dioxide levels in the earth's early atmosphere. *Science* **1986**, *234*, 1383–1385.
60. Karran, P.; Lindahl, T. Hypoxanthine in deoxyribonucleic acid: generation by heat-induced hydrolysis of adenine residues and release in free form by a deoxyribonucleic acid glycosylase from calf thymus. *Biochemistry* **1980**, *19*, 6005–6011. Quantifies the rate of spontaneous deamination of adenine to hypoxanthine in single-stranded DNA at 110 degrees Celsius ($k = 4 \times 10^{-8} \text{ s}^{-1}$), relevant for prebiotic chemistry and DNA damage, <https://doi.org/10.1021/bi00567a008>.
61. Dong, C.; Jin, M.; Lingam, M.; Airapetian, V.S.; Ma, Y.; van der Holst, B. Atmospheric escape from the TRAPPIST-1 planets and implications for habitability. *Proceedings of the National Academy of Sciences* **2018**, *115*, 260–265, [<https://www.pnas.org/doi/pdf/10.1073/pnas.1708010115>]. <https://doi.org/10.1073/pnas.1708010115>.
62. Tabataba-Vakili, F.; Grenfell, J. L.; Grießmeier, J.-M.; Rauer, H.. Atmospheric effects of stellar cosmic rays on Earth-like exoplanets orbiting M-dwarfs. *A&A* **2016**, *585*, A96. <https://doi.org/10.1051/0004-6361/201425602>.
63. Tilley, M.A.; Segura, A.; Meadows, V.; Hawley, S.; Davenport, J. Modeling Repeated M Dwarf Flaring at an Earth-like Planet in the Habitable Zone: Atmospheric Effects for an Unmagnetized Planet. *Astrobiology* **2019**, *19*, 64–86, [[arXiv:astro-ph/EP/1711.08484](https://arxiv.org/abs/astro-ph/EP/1711.08484)]. <https://doi.org/10.1089/ast.2017.1794>.
64. Cox, A.N.; Pilachowski, C.A. *Allen's Astrophysical Quantities*, 4th ed.; Springer: New York, 2000. Standard reference for stellar parameters, including main-sequence lifetimes for O through M stars.
65. Laughlin, G.; Bodenheimer, P.; Adams, F.C. The End of the Main Sequence. *Astrophys. J.* **1997**, *482*, 420–432. Estimates main-sequence lifetimes for low-mass stars, particularly K and M dwarfs, up to 10^{14} years for M5V, <https://doi.org/10.1086/304125>.
66. Cox, A.N., Ed. *Allen's Astrophysical Quantities*, 4th ed.; Springer: New York, 2000. Comprehensive data on stellar masses and lifetimes, used for all spectral types.
67. Schaller, G.; Schaerer, D.; Meynet, G.; Maeder, A. New Grids of Stellar Models from 0.8 to 120 Solar Masses at $Z = 0.020$ and $Z = 0.001$. *Astron. Astrophys. Suppl. Ser.* **1992**, *96*, 269–331. Provides stellar evolution tracks for high-mass stars, used for O and B star lifetimes.
68. Allwood, A.C.; Walter, M.R.; Kamber, B.S.; Marshall, C.P.; Burch, I.W. Stromatolite reef from the Early Archaean era of Australia. *Nature* **2006**, *441*, 714–718. Provides evidence of stromatolites and microbial activity in the Strelley Pool Formation, dated to 3.43 Ga, representing the earliest widely accepted evidence of bacterial life on Earth, <https://doi.org/10.1038/nature04764>.
69. Schwertner, E.W.; Leung, M. An Overview of Exoplanet Biosignatures. *Reviews in Mineralogy and Geochemistry* **2024**, *90*, 465–514. <https://doi.org/10.2138/rmg.2024.90.13>.
70. Schwertner, E.W.; Kiang, N.; Parenteau, M.; Harman, C.; DasSarma, S.; Fisher, T.; Arney, G.; Hartnett, H.; Reinhard, C.; Olson, S.; et al. Exoplanet Biosignatures: A Review of Remotely Detectable Signs of Life. *Astrobiology* **2018**, *18*, 663–708. <https://doi.org/10.1089/ast.2017.1729>.